EFFECT OF PRESSURE GRADIENT ON CAVITATION INCEPTION FROM AN ISOLATED SURFACE ROUGHNESS

Masaru Tada

Technical Memorandum
File No. TM 82-218
18 October 1982
Contract No. N00024-79-C-6043

Copy No. 13

The Pennsylvania State University
Intercollege Research Programs and Facilities
APPLIED RESEARCH LABORATORY
Post Office Box 30
State College, PA 16801

NAVY DEPARTMENT

NAVAL SEA SYSTEMS COMMAND

UNCLASSIFIED

SECURITY CLASSIFICATION OF THIS PAGE (When Data Entered)

REPORT DOCUMENTATION PAGE	READ INSTRUCTIONS BEFORE COMPLETING FORM
1. REPORT NUMBER: TM 82-218	2. GOVT ACCESSION NO.: AD-A129 999
	3. RECIPIENT'S CATALOG NUMBER: 8
4. TITLE (and Subtitle): EFFECT OF PRESSURE GRADIENT ON CAVITATION INCEPTION FROM AN ISOLATED SURFACE ROUGHNESS	5. TYPE OF REPORT & PERIOD COVERED: Technical Memorandum
	6. PERFORMING ORG. REPORT NUMBER
7. AUTHOR(s): Masaru Tada	8. CONTRACT OR GRANT NUMBER(s): N00024-79-C-6043
9. PERFORMING ORGANIZATION NAME AND ADDRESS: Applied Research Laboratory Post Office Box 30 State College, PA 16801	10. PROGRAM ELEMENT, PROJECT, TASK AREA & WORK UNIT NUMBERS
11. CONTROLLING OFFICE NAME AND ADDRESS: Naval Sea Systems Command, Code NSEA-63R31 Washington, DC 20362	12. REPORT DATE: 18 October 1982
	13. NUMBER OF PAGES: 106
14. MONITORING AGENCY NAME & ADDRESS (if different from Controlling Office)	15. SECURITY CLASS. (of this report): Unclassified
	15a. DECLASSIFICATION/DOWNGRADING SCHEDULE

16. DISTRIBUTION STATEMENT (of this Report)

Approved for public release. Distribution unlimited.
Per NAVSEA - Nov. 23, 1982

17. DISTRIBUTION STATEMENT (of the abstract entered in Block 20, if different from Report)

18. SUPPLEMENTARY NOTES

19. KEY WORDS (Continue on reverse side if necessary and identify by block number)

thesis, pressure, gradient, inception, surface, roughness

20. ABSTRACT (Continue on reverse side if necessary and identify by block number)

An experimental investigation was conducted to study the cavitation characteristics of different triangular protrusions in the presence of a pressure gradient. The shape factor (G) and wake parameter (Π) were calculated from a pressure gradient and the boundary layer parameters with

DD FORM 1 JAN 73 1473 EDITION OF 1 NOV 65 IS OBSOLETE

UNCLASSIFIED

SECURITY CLASSIFICATION OF THIS PAGE (When Data Entered)

the assistance of computer programs based on the method of E. Truckenbrodt. Limited cavitation numbers were obtained visually for the flow with different cases of zero, favorable and unfavorable pressure gradient. For the case of zero pressure gradient, a power law relationship was established between the limited cavitation number ($\sigma_{\ell fp}$) and the relative height (h/δ) and Reynold's number based on boundary layer thickness ($\frac{U\sigma}{\nu}$). In addition, the comparison of the power law obtained by the present investigation with that by Holl [29] was carried out. Furthermore, a development of the characteristic velocity theory was made semi-empirically. For a flow with pressure gradient, the power law relationship was extended to include the influence of shape factor (G). This extended power law in which $\sigma_{\ell fp}$ is correlated with $\frac{h}{\delta}$, $\frac{U\delta}{\nu}$, and G is shown to be in good agreement with experimental data.

Subject: M.S. Thesis by Masaru Tada

Abstract: This memorandum contains the abstract of a thesis entitled "Effect of Pressure Gradient on Cavitation Inception from an Isolated Surface Roughness". This thesis is to be submitted to the Graduate School in partial fulfillment of the requirements for the M.S. Degree in Aerospace Engineering. The anticipated graduation date is March 1983. This work was supervised by Drs. Michael L. Billet and J. William Holl and was supported by NAVSEA Code 63R61.

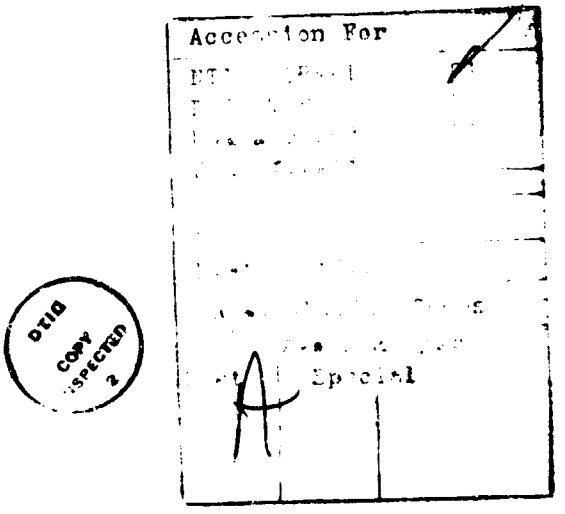

ABSTRACT

An experimental investigation was carried out for the case of different triangular protrusions, to study the cavitation characteristics in the presence of a pressure gradient. The shape factor (G) and wake parameter (Π) were calculated from the pressure gradient and the boundary layer parameters with the assistance of computer programs based on the method of E. Truckenbrodt. Limited cavitation numbers were obtained visually for the flow with different cases of zero, favorable and unfavorable pressure gradient. For the case of zero pressure gradient, a power law relationship was established between the limited cavitation number (σ_{crit}) and the relative height (h/δ) and Reynold's number based on boundary layer thickness ($\frac{u\delta}{\nu}$). In addition, the comparison of the power law obtained by the present investigation with that by Holl [29] was carried out. Furthermore, a development of the characteristic velocity theory was made semi-empirically. For a flow with pressure gradient, the power law relationship was extended to include the influence of shape factor, (G).

TABLE OF CONTENTS

Page

LIST OF TABLES

LIST OF FIGURES

LIST OF SYMBOLS

a,b,c,d,e	Constants in cavitation law
B	Constant in universal velocity law
C	Chord length
C_f	Skin friction coefficient, $C_f = \tau_w/\rho\frac{U^2}{2}$
C_p	Pressure coefficient
$C_{p_{min}}$	Minimum pressure coefficient
$C_{p_{min-o}}$	Minimum pressure coefficient of the irregularity in rotational flow on a flat plate
$C'_{p_{min-o}}$	Minimum pressure coefficient of the irregularity in irrotational flow on a flat plane
$C_{p_{min-R}}$	Minimum pressure coefficient of the parent body with roughness
C_{p_s}	Pressure coefficient for the smooth parent body
G	Boundary layer shape factor
h	Isolated roughness height
H	Boundary layer shape factor, $H = \delta^*/\theta$
$\overline{H}$	Boundary layer shape factor $\overline{H} = \delta^{**}/\theta$
k	Von Kármán's constant
ℓ	A mixing length
L	Boundary layer shape factor $L = \int\frac{d\overline{H}}{(h-1)\overline{H}}$
L_c	Characteristic length of the flow about the irregularity
M	Exponent in velocity power law
P	Pressure
P_{min}	Minimum pressure
P_{min-R}	Minimum pressure at the irregularity in rotational flow

P'_{min-R}	Minimum pressure at the irregularity in irrotational flow
P_v	Vapor pressure
P_∞	Pressure at infinity for the parent body
P_o	Pressure far upstream of the infinity point
P_{min-r}	Minimum pressure produced by the roughness
$P_{\infty\ell}$	Pressure at infinity for limited cavitation
Re_h	Reynolds number based on roughness height
Re_δ	Reynolds number based on boundary layer thickness
$\overline{u}$	Mean velocity
U_c	Characteristic velocity of the flow about the irregularity
u'	Fluctuating velocity
u_*	Friction velocity
U_∞	Velocity at infinity for the parent body (Fig. 3-3 or as shown in Fig. 5-1)
U_{max}	Maximum velocity in the approximate rotational flow about the irregularity
U'_{max}	Maximum velocity in the irrotational flow about the irregularity
U	Local velocity at edge of the boundary layer
v'	Instantaneous velocity in y direction
W	Wake function
x	Coordinate in streamwise direction
y	Coordinate normal to flow
α	Gas content
β	Claussec's equilibrium parameter
β'	Henry's law constant

δ	Boundary layer thickness
δ^*	Displacement thickness
δ^{**}	Energy thickness
θ	Momentum thickness
μ	Viscosity
μ_+	Eddy viscosity
ν	Kinematic viscosity
Π	Wake parameter
ρ	Mass density of the liquid
σ_i	Incipient cavitation number
σ_d	Desinent cavitation number
σ_ℓ	Limited cavitation number
$\sigma_{\ell R}$	Limited cavitation number for roughened body
$\sigma_{\ell fp}$	Limited cavitation number under essentially flat plate conditions
$\sigma'_{\ell fp}$	Same as $\sigma_{\ell fp}$ for roughness in the absence of a boundary layer
τ_w	Wall shear stress
τ_t	Reynolds stress
Ω	Bubble dynamic effect for cavitation number

ACKNOWLEDGMENTS

I would like to express my appreciation to Dr. Michael L. Billet and Dr. J. William Holl for their patience and guidance during the course of this study. In addition, I would like to thank all of the individuals at the Applied Research Laboratory who contributed in many ways to this study. In particular, I would like to thank Mr. Allen L. Treaster, Research Assistant, for his numerous helpful suggestions and actions in the final processing of this thesis.

The investigation was conducted in the Fluids Engineering Department (FED) of the Applied Research Laboratory, The Pennsylvania State University. The research was conducted in the 4.5-inch x 20-inch water tunnel which is located in the Garfield Thomas Water Tunnel Building and was sponsored by the Naval Sea System Command, Code 63R31.

CHAPTER I

INTRODUCTION

1.1 Fundamental Characteristics of Cavitation

When the local pressure falls below a critical value, small bubbles grow by vaporization or by degassing. Bubble growth by vaporization is called vaporous cavitation if caused by dynamic pressure reduction at essentially a constant temperature. For vaporous cavitation, which is of primary interest, the critical value of pressure is less than or equal to the vapor pressure of the liquid. In the initial steps of the phenomenon, microbubbles grow in the minimum pressure region and then when transferred to higher pressure regions by the fluid flow, the growth will be arrested. The collapse of bubbles will cause material damage, noise and vibration.

On the other hand, a further reduction in the minimum pressure will promote the growth of bubbles and may result in large cavities attached to the body. The succeeding stages are distinguished from the initial stage by the term developed cavitation, which may produce a serious performance loss when it occurs on hydromachinery, marine vehicles, etc.

1.2 The Effect of the Surface Irregularities on Cavitation

Basically, surface irregularities may be divided into two categories, namely, isolated and distributed.

Isolated irregularities will cause high local velocities, low pressures and turbulence in the neighborhood of the projection.

Distributed irregularities will change velocities, pressure and turbulence generally throughout the volume of boundary layer fluid. Surface irregularities, therefore, advance the onset of cavitation on a body and reduce its design performance. In general, isolated irregularities are more harmful to cavitation performance than distributed irregularities because the local pressure reduction is more severe.

1.3 Thesis Objectives

The objective of this thesis is to investigate the effect of pressure gradient on the cavitation inception of an isolated irregularity. In so doing, a curved wall element was attached on one wall in the water tunnel test section, and triangular protrusions of various sizes were mounted on the opposite side as isolated irregularities. In order to attain the objective, the velocity profiles of the boundary layer and the pressure gradient were measured in the initial phase of the test and then subsequently the cavitation number was measured for the cases in which the tip of the triangular protrusion was both inside and outside the boundary layer.

CHAPTER II

PREVIOUS INVESTIGATIONS

2.1 The Influence of Irregularities on Cavitation

Surface irregularities are one of the major factors influencing cavitation inception. Recent requirements of compact and high speed hydromachinery have demanded more extensive knowledge of the effect of irregularities on cavitation.

The initial work in this area was concerned with performance losses in turbomachinery. Shalnev [1] studied cavitation caused by surface irregularities in the clearance between the pump blades and the casing wall. However, his results would only be applicable to similar boundaries since they were not correlated with boundary layer parameters.

Walker [2] employed the concept of relative height of roughness (h/δ), where h is the height of roughness and δ the local boundary layer thickness. However, his investigation was conducted for specific conditions and was not done systematically.

Holl [3,4] systematically investigated cavitation inception numbers for two dimensional isolated roughness elements, namely, circular arcs and sharp edged triangular strips on a flat plate. By placing the roughness at different locations in the boundary layer of a smooth wall, he found that the cavitation number could be correlated with the relative height of roughness (h/δ), a Reynolds number (Re_n) based on roughness height and local velocity, and the ordinary Kármán-Pohlhausen type shape factor (H).

Benson [5] investigated cavitation inception numbers for three-dimensional isolated roughness elements, namely, hemispheres, cones, and circular cylinders on a flat plate. He showed that the cavitation correlated well with a local Reynolds number based on the roughness height and the flow velocity at the height of the roughness.

The effect of distributed roughness on cavitation is more complicated than the case of an isolated roughness because there is an interrelation between the boundary layer development and the degree of surface roughness. However, several studies have been conducted since the first publication to appear regarding distributed roughness by Benson [6].

The classical work in distributed roughness is that of Arndt [7] and Arndt and Ippen [8]. From an examination of the results compiled by Benson [6], Arndt indicated that the cavitation occurring in the roughness grooves was probably of the gaseous type, and the cavitation occurring in the boundary layer was vaporous cavitation. Arndt and Ippen studied the effect of distributed roughness by experiments with triangular groove irregularities. They showed that cavitation occurred in the middle of the boundary layer, and correlated the incipient cavitation number (σ_i) with the wall shear stress coefficient (C_f) for the rough boundary.

Additional studies concerned with distributed roughness on cavitation are (1) experiments with sand grain irregularities by Messenger [9] and Huber [10]; (2) experiments with wire screen irregularities by Bechtel [11], and (3) the effect of surface roughness on the performance of hydrofoils by Numachi et al. [12,13]. The investigations by Messenger,

Huber and Bechtel confirmed the linear relationship between σ_i and C_f which was established by Arndt [7] and Arndt and Ippen [8].

2.2 Velocity Profiles of Boundary Layers

The velocity profiles for turbulent boundary layers may be divided into three parts:

1) Inner layer

2) Outer layer

3) Overlap layer.

For the inner layer, dominated by viscous shear, Prandtl [14] deduced that the mean velocity ($\overline{u}$) must depend upon the wall shear stress, the fluid properties, and the distance (y) from the wall. Thus, he proposed the inner law or so-called law of the wall:

$$\overline{u} = f(\tau_w, \rho, \mu, y), \tag{2-1}$$

where τ_w is the shear stress at the wall.

For the outer layer, dominated by turbulent shear, Von Kármán [15] deduced that the wall tends to act merely as a source of retardation, reducing the local velocity ($\overline{u}$) below the freestream value (U) in a manner which is independent of viscosity (μ) but dependent upon the shear stress at the wall and the distance (y) over which its effect has diffused. Thus, he proposed the outer, or velocity defect, law:

$$U - \overline{u} = f(\tau_w, \rho, y, \delta), \tag{2-2}$$

where δ is the boundary layer thickness.

For the overlap layer, Millikan [16] simply specified that the two functions merge together smoothly over some finite region between the inner and outer layer.

From dimensional analysis, the non-dimensional form of the law of the wall and the velocity defect law, respectively, are

$$\frac{\bar{u}}{u_*} = f\left(\frac{\rho u_* y}{\mu}\right) \tag{2-3}$$

and

$$\frac{U - \bar{u}}{u_*} = g\left(\frac{y}{\delta}\right) \tag{2-4}$$

where

$$u_* = \sqrt{\frac{\tau_w}{\rho}} \, . \tag{2-5}$$

In the overlap layer, a velocity profile can be expressed by using a mixing length model. The Reynolds stress in turbulent flow is expressed as,

$$\tau_t = C \rho \ell^2 \frac{\partial \bar{u}}{\partial y}\left|\frac{\partial \bar{u}}{\partial y}\right| , \tag{2-6}$$

where ℓ is a mixing length and C is a coefficient of order one. This is called Prandtl's mixing-length hypothesis. The eddies involved in momentum transfer have characteristic vorticities of order v'/ℓ and they maintain their vorticity because of their interaction with the mean shear $(\frac{\partial \bar{u}}{\partial y})$, so that

$$\frac{v'}{\ell} \sim \frac{\partial \bar{u}}{\partial y} \, , \tag{2-7}$$

where v' is the instantaneous velocity in the y direction.

From equations (2-6) and (2-7)

$$\tau_t = \rho\, v'\, \ell \frac{\partial \bar{u}}{\partial y} . \tag{2-8}$$

On the assumption that u' and v' are well correlated, the Reynold's stress will be

$$\tau_t = \rho\, u_*^2, \tag{2-9}$$

where u' is the instantaneous velocity in the x direction and u_* is the wall-friction velocity.

From equations (2-8) and (2-9)

$$\frac{1}{u_*} \frac{\partial \bar{u}}{\partial y} = \frac{1}{k} \frac{1}{y} , \tag{2-10}$$

where k is a constant.

After integrating equation (2-10),

$$\frac{\bar{u}}{u_*} = \frac{1}{k} \ell n\ y + \text{const.} \tag{2-11}$$

Furthermore, equation (2-11) can be written as

$$\frac{\bar{u}}{u_*} = \frac{1}{k} \ell n \frac{y u_*}{\nu} + B,$$

where k is known as the constant of Von Kármán and B is an empirical constant. Nikuradse [17] in 1930 found that the constants k and B were 0.40 and 5.5 and Coles [18] in 1955 employed 0.41 and 5.0 for k and B, respectively.

2.3 The Law of the Wake for Turbulent Boundary Layers

The outer law is more sensitive to external parameters, particularly the pressure gradient, as shown in Fig. 6-4, p. 470 of Ref. [19].

Clauser [20,21] was the first investigator to introduce new parameters involving the pressure gradient for the outer layer; these are given by

$$\frac{U - \bar{u}}{u_*} = g\left(\frac{y}{\delta}, \frac{\delta}{\tau_w}\frac{dp}{dx}\right) . \tag{2-13}$$

After further investigation, he concluded that δ should be replaced by the displacement thickness. Therfore, the accepted parameter (β) is

$$\beta = \frac{\delta^*}{\tau_w}\frac{dp}{dx} . \tag{2-14}$$

A shape factor (G) which remains constant in an equilibrium boundary layer was defined by Clauser as

$$G = \frac{1}{\Delta}\int_0^\infty \left(\frac{U - \bar{u}}{u_*}\right)^2 dy, \tag{2-15}$$

where

$$\Delta = \int_0^\infty \frac{U - \bar{u}}{u_*}\, dy = \delta^*\sqrt{\frac{2}{C_f}} . \tag{2-16}$$

Equation (2-15) can be related to the ordinary Kármán-Pohlhausen type shape factor (H) by

$$G = \sqrt{\frac{2}{C_f}}\left(1 - \frac{1}{H}\right) . \tag{2-17}$$

The shape factor (H) is not constant in an equilibrium boundary layer because the skin friction varies with x. It is said that G is a better shape factor than H in terms of predicting the properties of equilibrium boundary layers. Nash [22] approximated G by using the pressure gradient

$$G \simeq 6.1 \sqrt{\beta + 1.81} - 1.7 \ . \qquad (2\text{-}18)$$

Furthermore, he noted that the outer layer has a wakelike structure and its eddy viscosity (μ_t) scaled with δ^* and U. Thus,

$$\mu_t \simeq K\rho U\delta^* \ , \qquad (2\text{-}19)$$

where K is a constant.

Mellor and Gibson [23] combined equations (2-13) and (2-19) into a theory of equilibrium wake profiles, which is in good agreement with experimental data, as shown in Fig. 6-7, p. 479 of Ref. [19]. The equilibrium concept is valid not only for positive values of β but also for negative β, as shown by Stratford [24], and Herring and Norbury [25], for example.

Coles [26] combined the wall component and the wake component with the wake function (W) and the wake parameter (Π) in order to express the velocity profile in the form

$$\frac{\bar{u}}{u^*} = \frac{1}{\kappa} \ln \frac{yu^*}{\nu} + B + \frac{\Pi}{k} W\left(\frac{y}{\delta}\right) \ . \qquad (2\text{-}20)$$

The wake function is normalized such that it is zero at the wall and attains a value of 2.0 at $y = \delta$. As shown by Coles, the wake function

is approximated by

$$W(\frac{y}{s}) \simeq 2 \sin^2(\frac{\Pi}{2} \frac{y}{\delta}) \quad , \tag{2-21}$$

which is quite accurate for routine use as shown in Fig. 6-8, p. 481 of Ref. [19]. The wake parameter derived by Coles and Hirst [27] is approximated by the empirical expression

$$\Pi \simeq 0.8 \ (\beta + 0.5)^{0.75} \quad . \tag{2-22}$$

This formula is arranged to fit the theoretical requirement of Mellor and Gibson [23] i.e., the wake must vanish at $\beta = -0.5$, corresponding to an asymptotically large favorable gradient. For a very large β, where there are no equilibrium data, the wake parameter was approximaced by the relation

$$\Pi \simeq 1 + 2.1 \sqrt{\beta} \quad . \tag{2-23}$$

CHAPTER III

PRELIMINARY CONSIDERATIONS

3.1 Definition of Cavitation Number

Cavitation is defined as the vapor and gas-filled voids occurring in a liquid when the local pressure falls below the vapor pressure, based on the bulk temperature of the fluid. The Euler number which describes this state may be written as

$$\sigma = \frac{P_\infty - P_v}{1/2\ V_\infty^2}, \qquad (3\text{-}1)$$

where σ is defined as the cavitation number, P_∞ and U_∞ are a reference pressure and velocity, respectively. The vapor pressure (P_v) and liquid mass density (ρ) correspond to the bulk temperature of the liquid.

The cavitation number is a valuable parameter in the correlation of cavitation data.

If σ is sufficiently large, there is no evidence of cavitation; whereas if σ is sufficiently small, the cavitation can be well developed. Limited cavitation occurs at an intermediate value of the cavitation number where the amount of cavitation is minimized. The cavitation number corresponding to this state is the limited cavitation number (σ_ℓ) given by

$$\sigma_\ell = \frac{P_{\infty\ell} - P_v}{1/2\ \rho\ U_\infty}. \qquad (3\text{-}2)$$

3.2 Incipient Cavitation and Desinent Cavitation

There are two ways to determine the cavitation number at a constant velocity in a water tunnel. The first method is to establish a velocity in the test section at a noncavitating condition and then decrease the tunnel pressure until cavitation occurs on the test element. The cavitation number thus determined is called the incipient cavitation number (σ_i). The second method is to establish a velocity in the test section at a condition of well-developed cavitation on the test element. The pressure is increased until the cavitation disappears. This method determines the desinent cavitation number (σ_d). Experience shows that σ_d is often more consistent than σ_i and tends to be the upper bound of σ_i. Therefore, in many cavitation experiments, σ_d is adopted as the limited cavitation number (σ_ℓ). Differences between incipient and desinent cavitation are due to cavitation hysteresis [28].

3.3 Analysis of Isolated Roughness

Isolated roughness may be divided into two categories, namely, streamlined or non-separating surface protrusions and separating such as a triangular element. For the former cases, cavitation occurs on the surface of the protrusion. For the latter case, cavitation occurs in the shear layer downstream from the point of separation.

The frozen-streamline theory (FST) developed by Holl [29,30] has been used to analyze the major characteristics of the flow about a two-dimensional nonseparated surface protrusion. Further an approximate method developed by Holl [4,29], which is called the characteristic velocity theory (CVT), was able to correlate the limited cavitation

number more successfully than FST, for a non-streamlined surface protrusion.

3.4 Characteristic Velocity Theory

Holl [4] developed the theory based on the assumption of frozen streamlines. The actual flow about the roughness element on a flat plate in rotational flow is shown in Figure 3-1. In order to gain a simple expression for the minimum pressure coefficient of the irregularity in rotational flow on a flat plate ($C_{p_{min\ o}}$) an approximate rotational flow is constructed and, in addition, a characteristic velocity (U_c) is introduced as shown in Fig. 3-2.

Between the flow at infinity along the wall and minimum pressure point, Bernoulli's equation is valid in the following form:

$$P + \frac{1}{2}\rho U_c^2 = P_{min\ R} + \frac{1}{2} U_{max}^2 . \qquad (3\text{-}3)$$

$C_{p_{min\text{-}o}}$ can be expressed in the form

$$C_{p_{min\text{-}o}} = \left(\frac{U_{max}}{U_\infty}\right)^2 - \left(\frac{U_c}{U_\infty}\right)^2 . \qquad (3\text{-}4)$$

If we assume that the shapes of the streamlines are the same in both the rotational and irrotational flow, then we can assume that

$$\left(\frac{U_c}{U}\right)^2 = \left(\frac{U_{max}}{U'_{max}}\right)^2 . \qquad (3\text{-}5)$$

Substitution of equation (3-5) into equation (3-4) results in

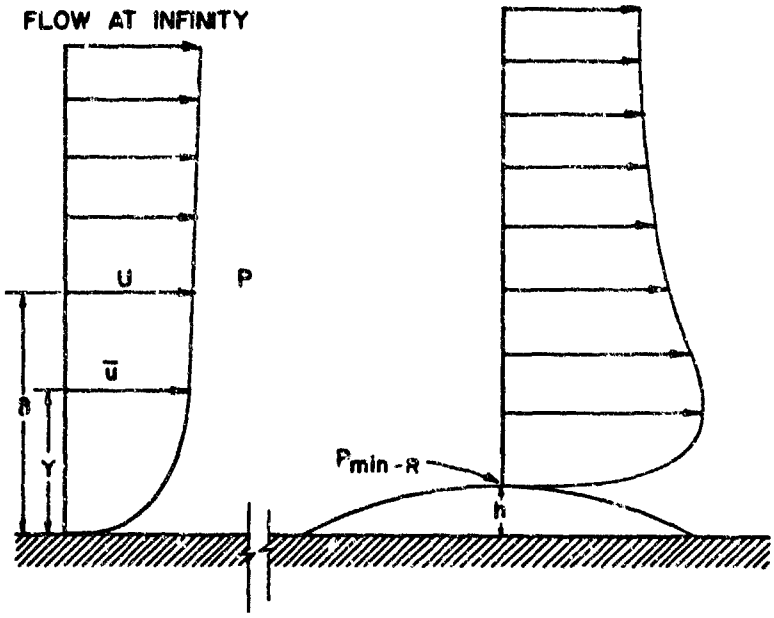

Figure 3-1. Rotational Flow about a Surface Irregularity on a Flat Plate.

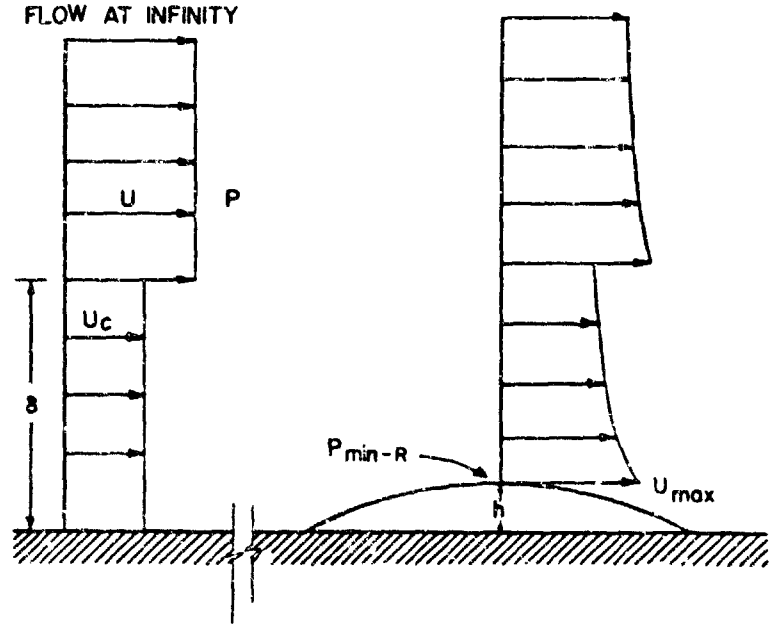

Figure 3-2. Approximate Rotational Flow about a Surface Irregularity on a Flat Plate.

$$C_{p_{min-o}} = \left(\frac{U_c}{U_\infty}\right)^2 C'_{p_{min-o}}, \tag{3-6}$$

where $C'_{p_{min-o}}$ is the minimum pressure coefficient of the irregularity in irrotational flow at a flat plate. If cavitation is assumed to occur at vapor pressure, i.e., that $P_{min-R} = P_v$, then the minimum pressure coefficient may be replaced by the limited cavitation number on a flat plate and equation (3-6) then becomes

$$\sigma_{\ell fp} = \left(\frac{U_c}{U_\infty}\right)^2 \sigma'_{\ell fp} \tag{3-7}$$

where $\sigma'_{\ell fp}$ is the limited cavitation number for the roughness in the absence of a boundary layer, that is $h/\delta = \infty$. Holl then assumed that U_c is the square root of the mean value of the square of the velocity upstream of the protrusion over some characteristic length, L_c. Holl assumed that L_c is equal to h so that

$$U_c = \sqrt{\frac{1}{h}\int_o^h u^{-2}\, dy}\,. \tag{3-8}$$

For turbulent flat plate boundary layers, power law velocity profiles are reasonable approximations to the actual velocity profiles at infinity except at the wall where the slope is infinite. Thu we have

$$\frac{\overline{u}}{U} = \left(\frac{y}{\delta}\right)^{\frac{1}{m}}. \tag{3-9}$$

Employing equation (3-8) in equation (3-7) for the power profiles yields

$$\sigma_{\ell fp} = \frac{1}{H} \left(\frac{h}{\delta}\right)^{\frac{2}{m}} \sigma'_{\ell fp} \quad \text{for} \quad \frac{h}{\delta} \leq 1 \tag{3-10}$$

and

$$\sigma_{\ell fp} = \left[1 - \frac{\delta}{h}\left(1 - \frac{1}{H}\right)\right]\sigma'_{\ell fp} \quad \text{for} \quad \frac{h}{\delta} \geq 1 \ . \tag{3-11}$$

The shape factor (H) defined as the ratio of the displacement thickness (δ^*) and the momentum thickness (θ) has the value

$$H = \frac{m+2}{m} \tag{3-12}$$

for the power law velocity profiles given by equation (3-9).

The theory may be employed to obtain a rough estimate of $\sigma_{\ell fp}$ for a separated protrusion element.

3.5 General Estimation of the Limited Cavitation Number on a Flat Plate for Isolated Roughness

We would expect that the cavitation number for an isolated roughness should be a function of the relative roughness (h/δ) and the boundary layer shape factor (H), from the frozen-streamline and characteristic velocity theories. In addition, Reynold's number (Re_h), based on the height of roughness, should be added to the function, according to the studies by Kermeen and Parkin [31], and Arndt [32]. Thus, we would expect the cavitation number for isolated roughness on a flat plate to have the general form

$$\sigma_{\ell fp} = f(\frac{h}{\delta}, H, Re_h) \tag{3-13}$$

which was proposed by Holl [29,30]. As a first approach, a simple power law equation for an isolated roughness on a flat plate may be given as

$$\sigma_{\ell fp} = C(\frac{h}{\delta})^a (\frac{U\delta}{\nu})^b \frac{1}{H^d}, \tag{3-14}$$

where C, a, b, and d are constants that depend on the shape of the irregularity.

3.6 Superposition Equation

Consider a surface irregularity located at some point on a parent body as shown in Fig. 3-3. The minimum pressure (P_{min-R}) occurs on the surface irregularity or in the wake of the irregularity if the flow is locally separating due to the roughness. The pressure difference $P_{min-R} - P_\infty$ can be written as

$$P_{min-R} - P_\infty = P - P_\infty + P_{min-R} - P \tag{3-15}$$

where P is the pressure in the vicinity of the roughness which may be thought of as the "local pressure at infinity" for the roughness element. Dividing equation (3-15) by $1/2\ \rho U_\infty^2$ yields

$$\frac{P_{min-R} - P_\infty}{1/2\ \rho U_\infty^2} = \frac{P - P_\infty}{1/2\ \rho U_\infty^2} + \frac{P_{min-R} - P}{1/2\ \rho U_\infty^2} (\frac{U}{U_\infty})^2 \tag{3-16}$$

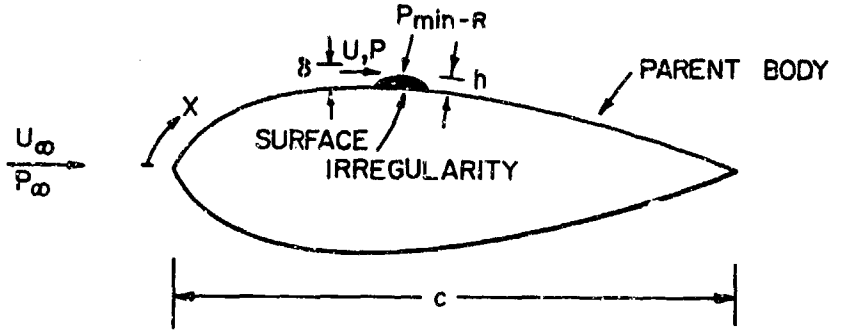

Figure 3-3. A Surface Irregularity on a Parent Body.

where U is the velocity at the edge of boundary layer in the vicinity of roughness which may be thought of as the "local velocity at infinity" for the surface irregularity. In terms of pressure coefficients, equation (3-16) can be written in the following form

$$C_{p_{min-R}} = C_{ps} + (1-C_{ps})C_{p_{min-o}} \quad . \tag{3-17}$$

Furthermore, if cavitation is assumed to occur at vapor pressure, then the minimum pressure coefficients may be replaced by cavitation numbers and equation (3-17) then becomes

$$\sigma_{\ell R} = - C_{ps} + (1-C_{ps})\, \sigma_{\ell fp} \quad . \tag{3-18}$$

This is the so-called superposition equation and was derived by Holl [29].

The equation is very useful in estimating the cavitation performance of a hydronautical body with surface irregularities, provided the smooth-body pressure coefficients (C_{ps}) and the limited cavitation number of the surface irregularity on a flat plate ($\sigma_{\ell fp}$) are known.

This equation has been revised by Arndt, Holl, Bohn, and Bechtel [33] to include possible bubble dynamic effects. The revised equation is

$$\sigma_{\ell R} = C_{ps} - \Omega + (1-C_{ps})\, \sigma_{\ell fp} \quad . \tag{3-19}$$

The function Ω accounts for possible bubble dynamic effects and is defined as

$$\Omega = \frac{P_v - P_{min-r}}{1/2\ \rho U_\infty^2} \qquad (3\text{-}20)$$

where P_{min-r} is the minimum pressure produced by the roughness.

CHAPTER IV

EXPERIMENTAL EQUIPMENT AND PROCEDURES

4.1 General Description of Water Tunnel

The experiments in this study were performed in the Garfield Thomas Water Tunnel Building of the Applied Research Laboratory located at The Pennsylvania State University. The 12-inch diameter water tunnel facility was designed to accommodate circular (12-inch) and rectangular (4.5-inch x 20-inch) test sections. A general view of this facility is shown in Fig. 4-1. The rectangular test section, shown in Fig. 4-2 and Fig. 4-3, was used throughout this study.

The flow velocity can be changed from 10 to 70 fps by a variable speed mixed-flow pump. The pressure in the test section can be varied from 3 to 60 psia by means of a partially filled water tank having an air chamber on top and connected to the tunnel circuit at the bottom. Alterations of the air pressure in the tank changes the pressure in the entire system.

The gas content was controlled by using a Cochrane Cold-Water Degasifier located in a bypass circuit. The system can decrease the total gas content to 2 moles of air per 10^6 moles of water (PPM).

For more detailed information, see reference [34].

4.2 Details of the Test Configurations

The experimental arrangement in the rectangular test section was composed of a triangular protrusion, the base for the protrusion and a curved-wall element. The test section fitted with two 10-inch by 20-inch

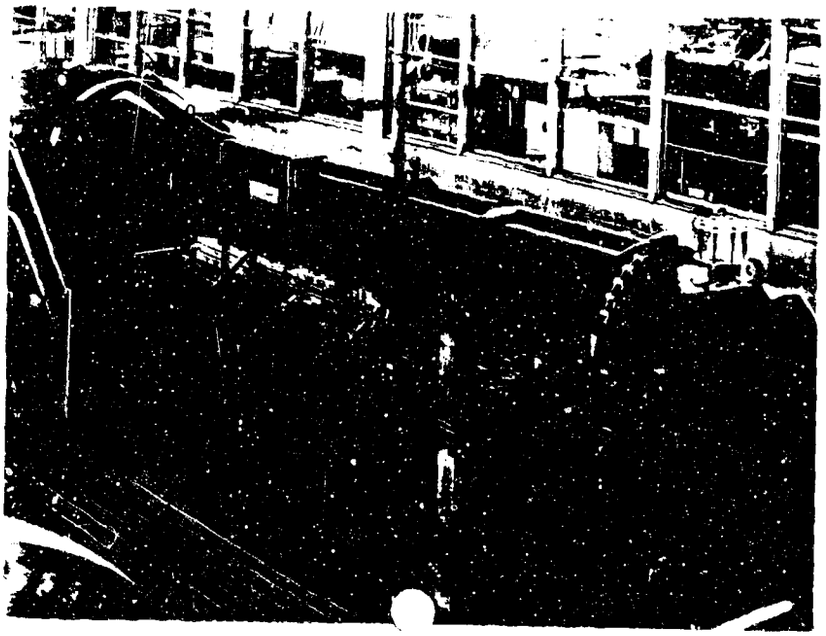

Figure 4-1. Photograph of the 4.5-Inch by 20-Inch Water Tunnel, Applied Research Laboratory.

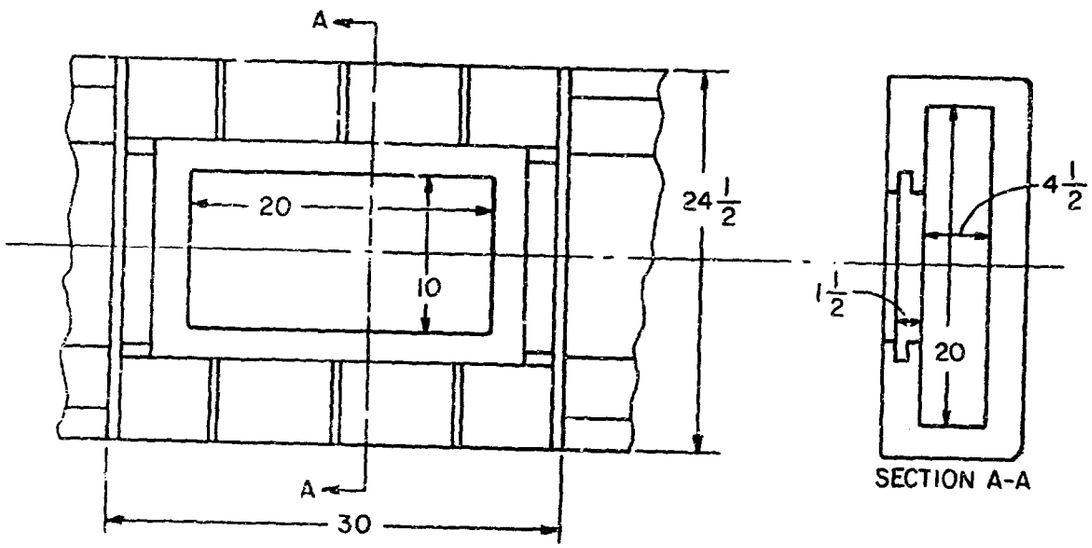

Figure 4-2. Rectangular Test Section.

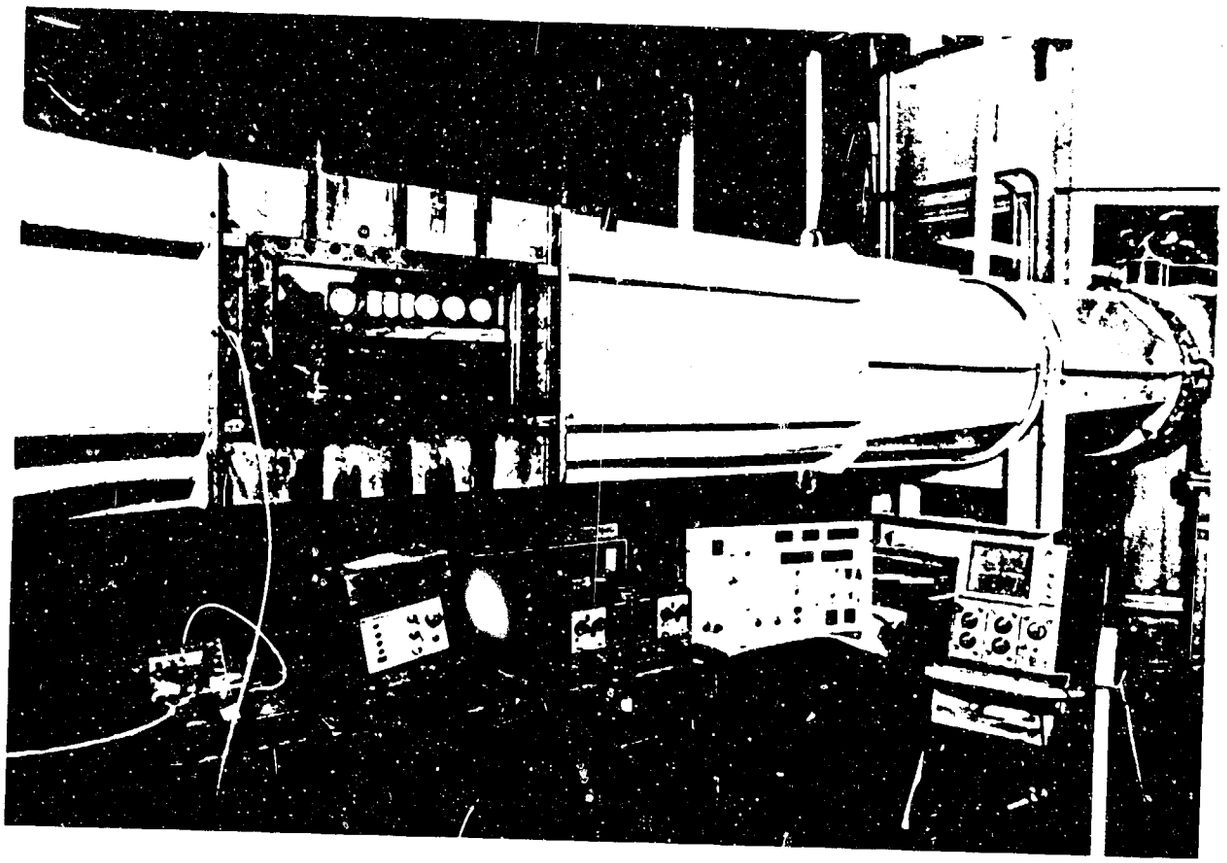

Figure 4-3. The 4.5-Inch by 20-Inch Test Section with Equipment.

plexiglass windows with an additional 2-inch by 20-inch window on the bottom panel. This arrangement is sketched in Fig. 4-4.

4.2.1 Curved Wall. The curved wall was made from plexiglass. The dimensions of the wall are shown in Fig. 4-5. In order to measure the velocity profiles at each location on the flat plate, seven holes were drilled in the wall for a total head tube. These locations are designated STA.I, II, III, IV, V, VI and VII, as shown in Fig. 4-6. Additional details of the design are presented in Appendix A.

4.2.2 Triangular Protrusion. The triangular protrusions used in this study were made from plexiglass. A photograph of the protrusion is shown in Fig. 4-7. The protrusions were of the same shape as those used by Holl [29]. Eight roughness heights were employed in the tests; namely, 1/100, 2/100, 3/100, 5/100, 7/100, 10/100, 15/100 and 30/100 inches and were mounted on the base one at a time for each experiment. The roughness locations correspond to the position of the leading edge of the total head tube. Additional details of the design are presented in Appendix A.

4.3 Measurement of the Velocity at Infinity in the Test Section

Infinity in the test section was defined as 6.40 inches upstream from the leading edge of the curved wall for all experiments. The velocity was determined by the difference between the static pressure at the infinity point with the curved wall (P'_∞) and the static pressure far upstream of the infinity point (P_o). The relationship between the static pressure difference ($P_o - P'_\infty$) and the dynamic pressure at infinity with the curved wall ($\frac{1}{2}\rho U'^2_\infty$) was measured three times by using a pitot tube. However, since cavitation occurred at the pitot

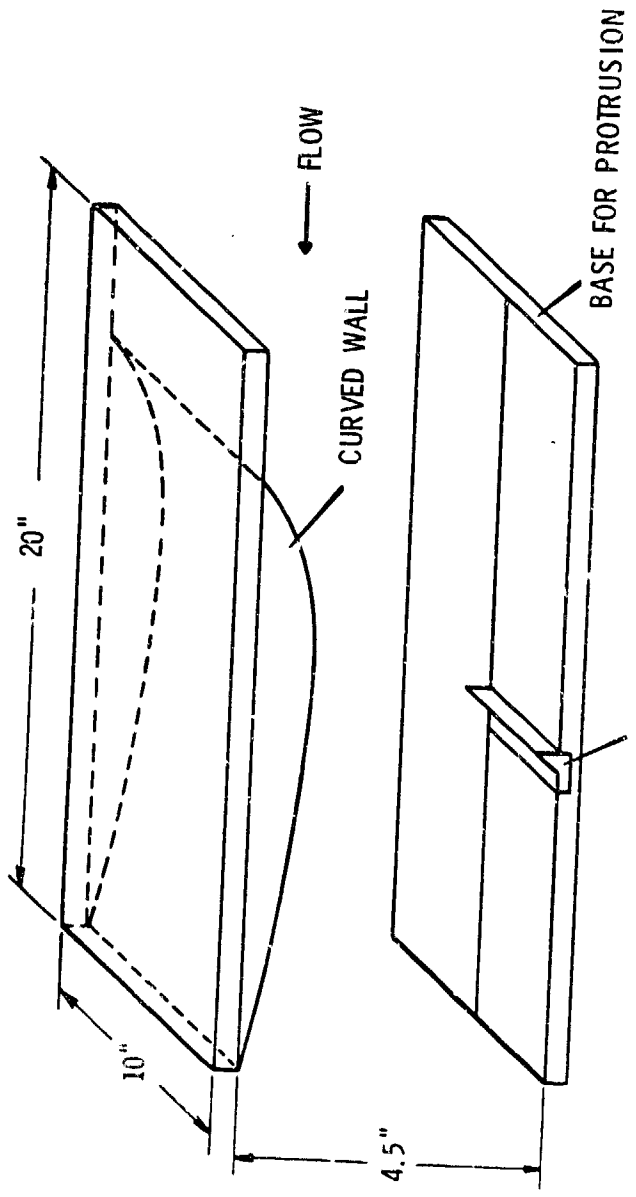

Figure 4-4. Isometric View of the Test Section.

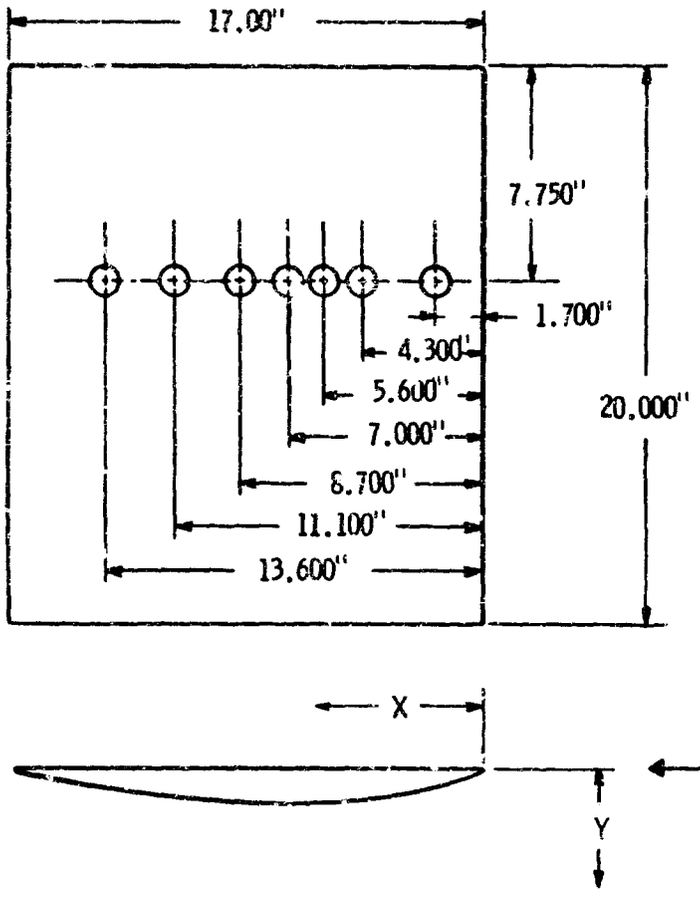

X (in.)	Y (in.)
0	0
0.213	0.128
0.425	0.190
0.850	0.283
1.275	0.355
1.700	0.414
2.550	0.509
3.400	0.577
5.100	0.657
6.800	0.680
8.500	0.660
10.200	0.603
11.900	0.508
13.600	0.376
15.300	0.212
16.150	0.116
17.000	0

Figure 4-5. Details of the Curved Wall.

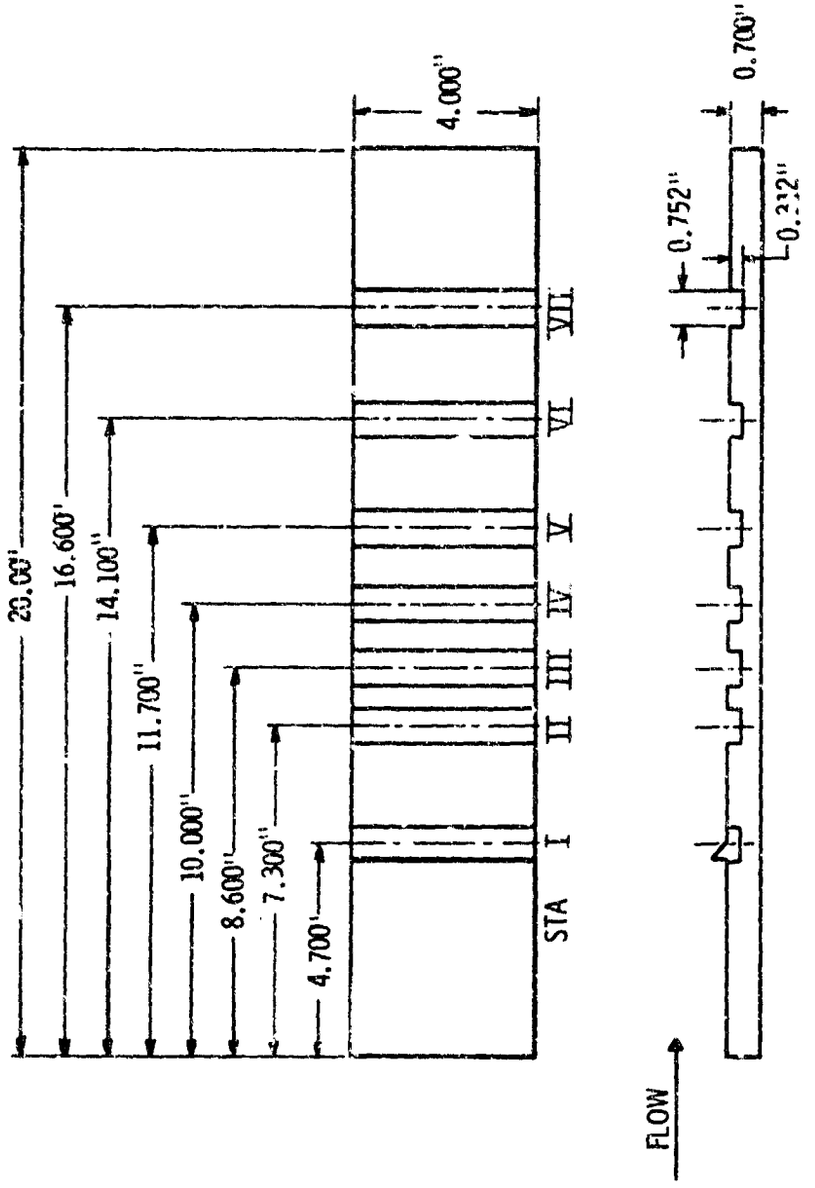

Figure 4-b. Position of the Triangular Protrusion.

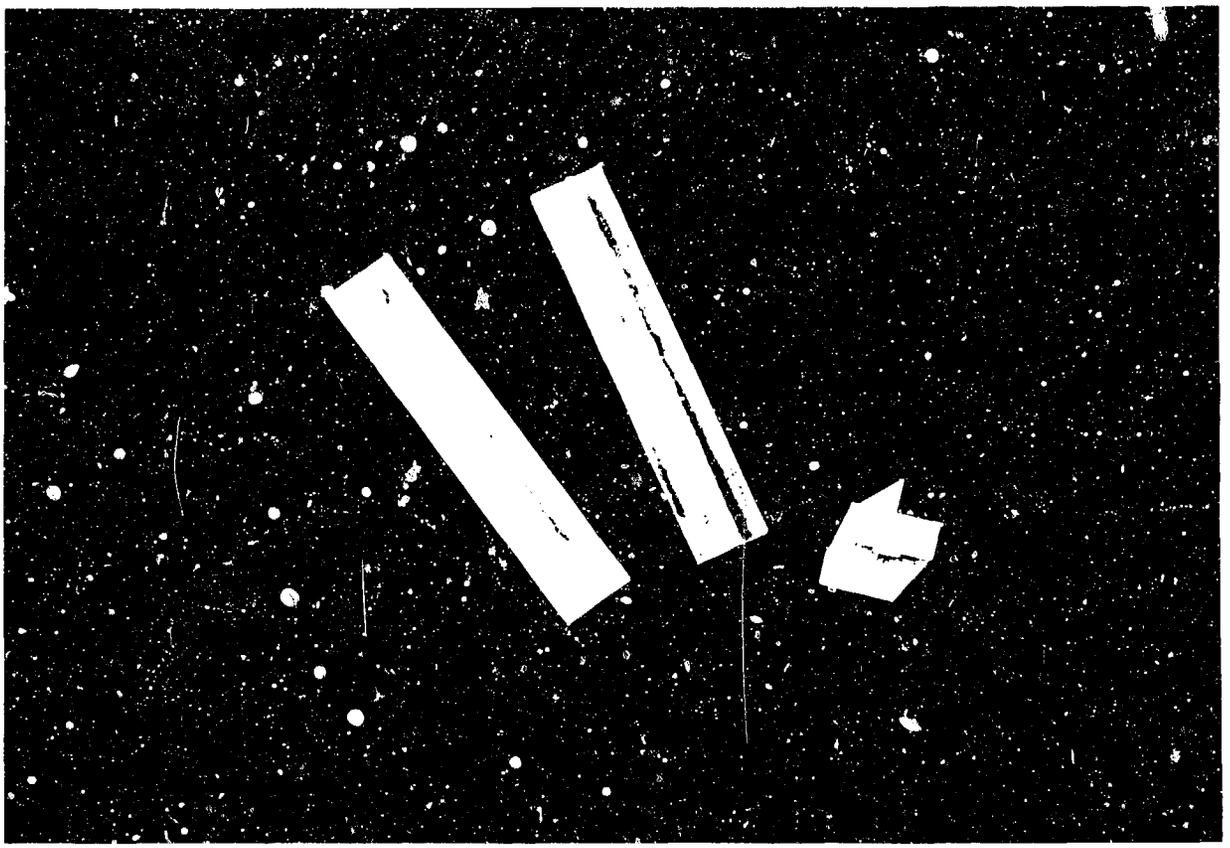

Figure 4-7. Photograph of the Triangular Protrusion.

tube for flow velocities greater than 40 fps, the measurements were obtained for velocities from 20 to 38 fps. The sketch of the measurement stations is shown in Fig. 4-8.

4.4 Measurement of the Pressure Coefficient

The pressure coefficients for the test section were determined by using a total head tube and the static taps on the flat plate. The static taps are located between the measuring stations on a smooth plexiglass plate, as shown in Fig. 4-9. The measurements by the total head tube and the static taps were not made at the same time because the flow is disturbed by the presence of a total head tube. First the static pressure at each station was measured for different flow velocities ranging from 20 fps to 60 fps and then the dynamic pressure at each station was measured.

4.5 Measurement of the Velocity Profile

Whenever the measurements of the mean velocity profile for each station were made, the positions at which the tip of the total head tube just touches the plate for both inward and outward movement of the traversers were carefully determined with the use of a microscope. This was essential in order to know the back-lash of the traversing gear and also to determine the initial measuring point. This procedure was of major importance in establishing accurate locations of the total head tube.

The velocity profiles were measured by traversing the boundary layer with a probe which was fabricated from a tube of rectangular cross section with an external size of 0.018 by 0.083 inches. The

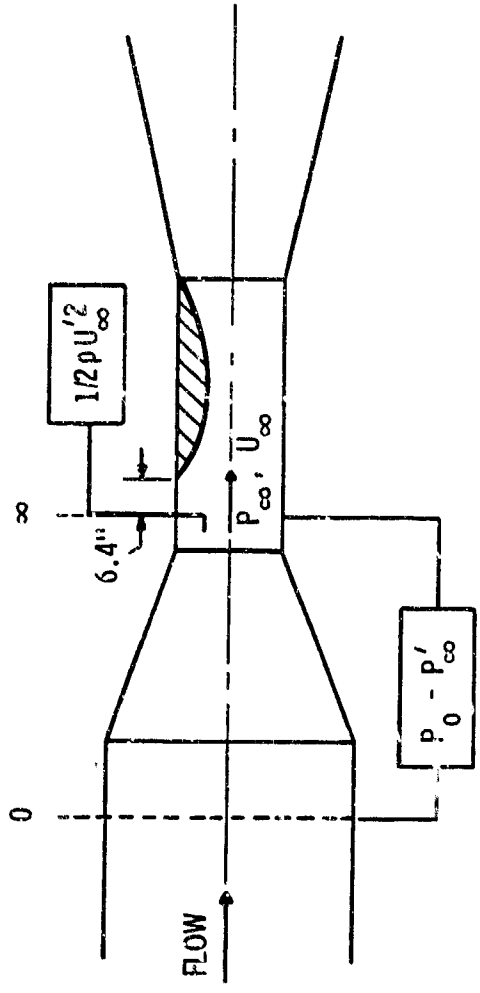

Figure 4-8. Schematic of the Measurement of the Velocity at Infinity.

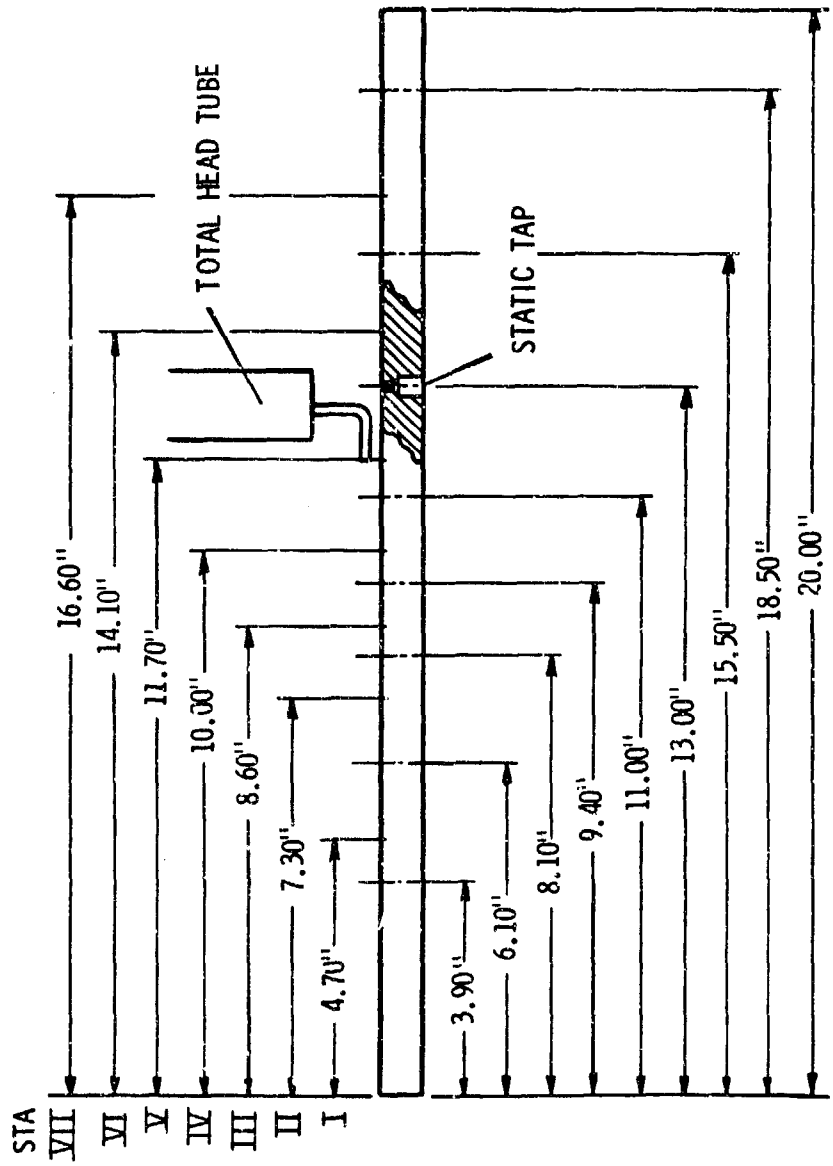

Figure 4-9. Location of Static Pressure Taps and Measurement Stations.

traversing device pictured in Fig. 4-10 allowed the positioning of the total head tube within 0.001 inch.

For each velocity profile, the total head tube position was zeroed on the plate and then moved outward in increments of 0.010 inch for a few initial measuring points, after which it was moved in steps of either 0.020 or 0.050 inch until the edge of the boundary layer was reached, in other words, until the total pressure became constant. The measurements were repeated as the tube was moved inward toward the wall in the same increments as employed in the outward motion. A third data set was obtained as the probe was again moved outwards. The final profiles were determined from the average of these three sets of data. While making measurements, the tunnel pressure was maintained at 40 psia and the water temperature was recorded before and after each profile run.

4.6 Visual Observation of Desinent Cavitation

Before observing cavitation, the gas content in the water tunnel was always measured. If the value was more than 4 p.p.m., purging the water of gas was done before the experiment by using the tunnel degasser. The gas content was measured by a "Thomas" Van Slyke Manometric Apparatus using a 10 cc sample.

As previously mentioned, there are two methods by which the critical cavitation number may be determined, i.e., inception and desinence. However, the desinence method was used to determine the limited cavitation number during the entire test because of repeatability.

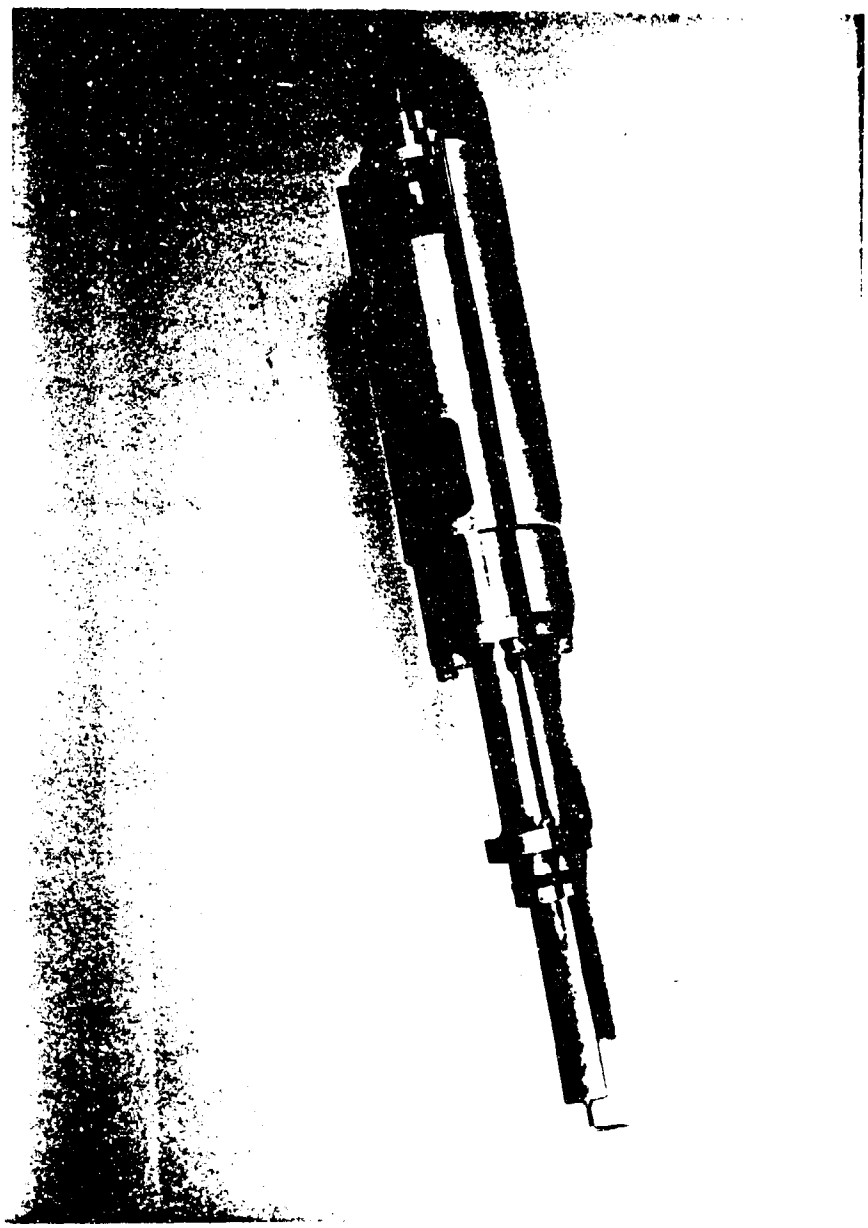

Figure 4-10. Photograph of Traversing Device and Total Head Tube.

At the start of the observation, a strobe light was used to aid in visually observing cavitation. When cavitation occurred along the top edge of the triangular protrusion, which appeared as luminous streaks originating several inches downstream of the protrusion, another type of cavitation appeared at both ends of the protrusion. These two types of cavitation joined together downstream. Special care was taken to see that the cavitation caused by the ends was not mistaken for that caused by the top edge of the protrusion.

Cavitation disappearance was defined as the absence of cavitation at the top edge of the protrusion, for less than 30 seconds. Throughout the experiment, the observations were done by the same person. The tunnel pressure was recorded at the defined infinity point. For each velocity setting, this pressure was lowered and raised seven times, with the final desinent cavitation number being based on the average pressure obtained by this procedure. In addition to the pressure measurements, the gas content and temperature were measured before and after each run. Since one side of the transducer was open to the atmosphere while taking the pressure measurements, it was necessary to record the barometric pressure several times each day.

A photograph of the cavitation phenomenon which occurred on the triangular protrusion is shown in Fig. 4-11.

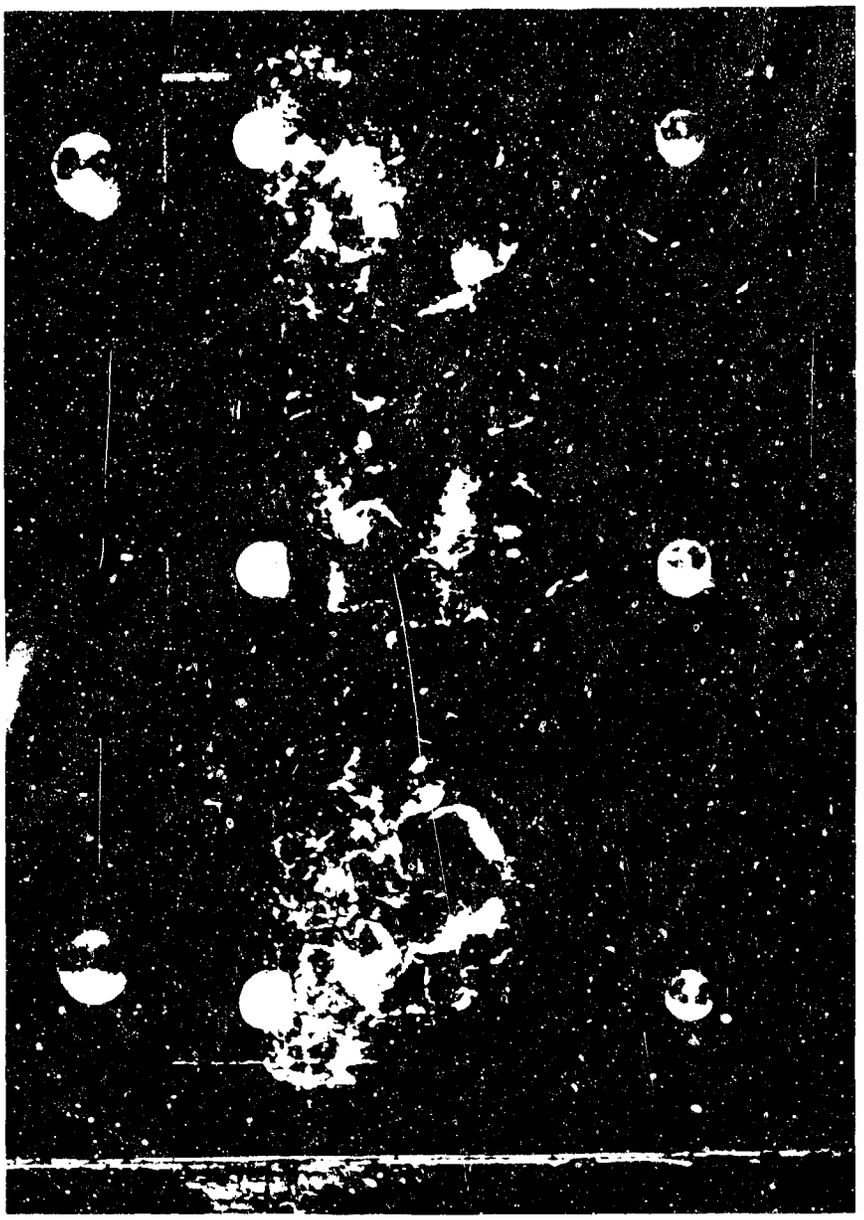

Figure 4-11. Photograph of Cavitation Phenomenon on a Triangular Protrusion.

CHAPTER V

PRESENTATION AND DISCUSSION OF RESULTS

5.1 Velocity at Infinity in the Test Section

As indicated previously, infinity in the test section was 6.40 inches upstream from the leading edge of curved wall (see section 4.3). The velocity at infinity cannot be measured directly by using the reference static pressure in the test section because of the presence of the curved wall in the test section.

The relationship between the static pressure difference $(P_o - P'_\infty)$ and the dynamic pressure at infinity $(1/2\ \rho U'^2_\infty)$ was empirically established from a set of experiments (see Fig. 4-8) and is of the form

$$1/2\ \rho U'^2_\infty = 0.9708\ (P_o - P'_\infty), \qquad (5\text{-}1)$$

where U' and P'_∞ are the velocity and pressure at infinity with the curved wall, respectively, as sketched in Fig. 5.1. The values of the dynamic pressure and static pressure difference are tabulated in Table 5.1.

The accuracy of the coefficient (0.9708) was investigated by applying Bernoulli's equation and also by utilizing the Douglas-Neumann computer program. The relationship between the dynamic pressure and static pressure without the curved wall can be established from Bernoulli's equation by knowing the ratio of cross-sectional area at the infinity point to that far upstream of the infinity point. Thus

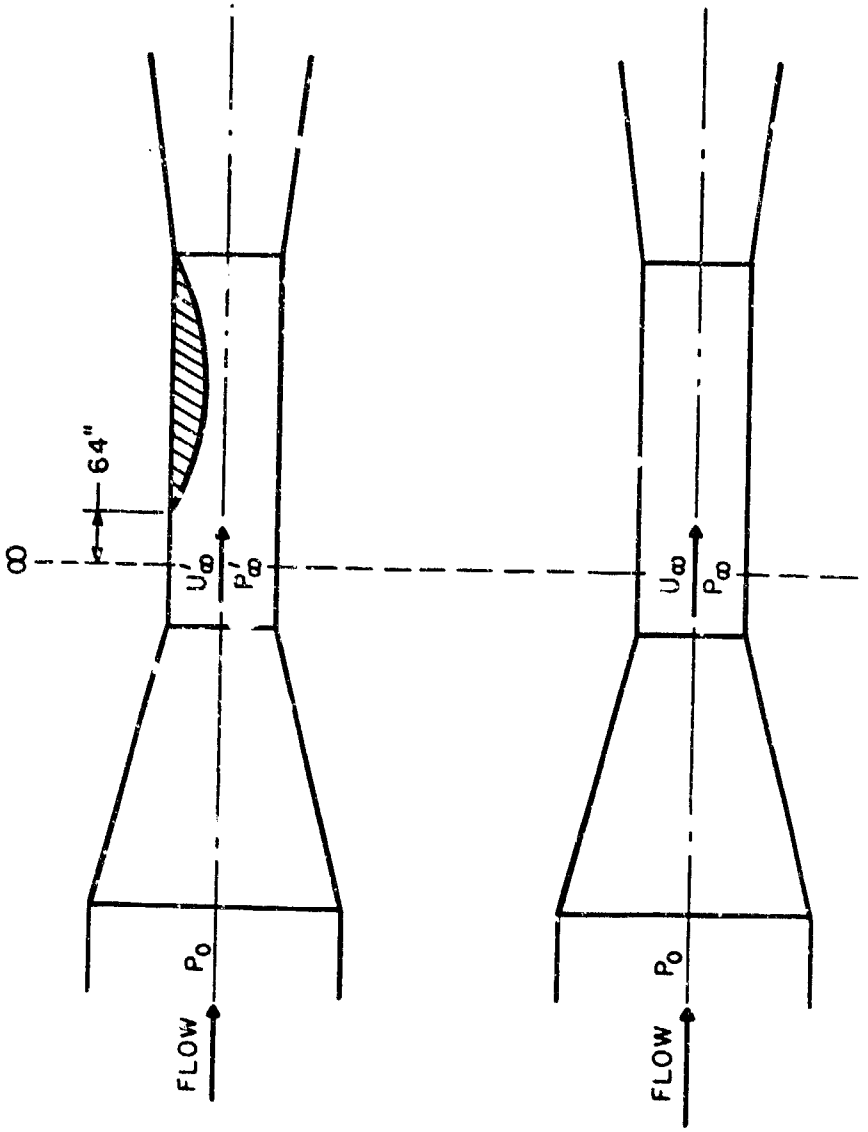

Figure 5-1. Sketch of the Velocity and Pressure at Infinity with and without the Curved Wall.

TABLE 5-1

RELATIONSHIP BETWEEN $1/2\rho U_\infty'^2$ AND $(P_o - P_\infty')$

DATA SET	1		2		3	
	$1/2\rho U_\infty'^2$ (volts)	$P_o - P_\infty'$ (volts)	$1/2\rho U_\infty'^2$ (volts)	$P_o - P_\infty'$ (volts)	$1/2\rho U_\infty'^2$ (volts)	$P_o - P_\infty'$ (volts)
Velocity (fps)						
20	0.9446	0.9850	0.9255	0.9780	-	-
23	1.2435	1.3165	1.2515	1.3230	1.2616	1.3610
25	1.4859	1.5537	1.5073	1.5715	1.5596	1.6580
28	2.0154	2.0850	2.0170	2.0912	1.9721	2.0800
30	2.3290	2.4206	2.3027	2.4085	2.3467	2.4400
33	2.7580	2.8450	2.7495	2.8650	2.6712	2.8113
35	3.0054	3.1231	3.0113	3.1460	2.9897	3.1320
38	3.4888	3.6240	3.5039	3.6250	3.4886	3.6300
$1/2\rho U_\infty'^2/P_o - P_\infty'$	0.9663		0.9693		0.9764	

Average value of $1/2\rho U_\infty'^2/P_o - P_\infty' = 0.9708$*

*Standard deviation = 0.0052

$$1/2\ \rho U_\infty^2 = 1.0079\ (P_o - P_\infty)\ . \qquad (5\text{-}2)$$

However, since the velocity at infinity is slightly affected by the presence of the curved wall, the modified velocity at infinity was calculated by the Douglas-Neumann computer program and the result is

$$\frac{U'_\infty}{U_\infty} = 0.9833\ . \qquad (5\text{-}3)$$

From equations (5-2) and (5-3), the relationship between the dynamic pressure and the static pressure difference can be expressed in the form

$$1/2\ \ U'^2_\infty = 0.9745\ (P_o - P_\infty)\ . \qquad (5\text{-}4)$$

It is felt that the coefficient (0.9708) in equation (5-1) is very accurate, because there is insignificant difference between equations (5-1) and (5-4). Hence, from equations (5-1) and (5-3), the relationship which was used during the entire experiment was obtained in the form of

$$1/2\ \rho U_\infty^2 = 1.0041\ (P_o - P_\infty)\ . \qquad (5\text{-}5)$$

5.2 Pressure Distribution and Gradient

The pressure coefficient in the test section is expressed as

$$C_p = \frac{P - P_\infty}{1/2\ \rho U_\infty^2}\ , \qquad (5\text{-}6)$$

where the static pressure (p) was measured at each station. Substituting

equation (5-5) into equation (5-6) yields

$$C_p = \frac{P - P_\infty}{1.0041\ (P_o - P_\infty)} \quad . \qquad (5\text{-}7)$$

In order to check the reliability of equation (5-7), the pressure coefficient was also calculated from the velocity at the edge of the boundary layer (U), shown in Fig. 5-2, which was measured by the total head tube. The pressure coefficient is expressed in the form of

$$C_p = 1 - \left(\frac{U}{U_\infty}\right)^2 \quad . \qquad (5\text{-}8)$$

As shown in Fig. 5-3, these pressure coefficients derived from equations (5-7) and (5-8) are in fairly good agreement. So the pressure coefficient obtained by using the static tap was used during the entire experiment and tabulated in Table 5-2.

However, in comparison with the calculated pressure coefficient which was used for designing the curved wall, the measured coefficients differ significantly. The difference between the experimental and calculated values is greater for the pressure gradient than for the pressure distribution. These two pressure gradients are shown in Fig. 5-4. Since STA. III and V have almost the same pressure gradient as that of STA. IV, the experiment for observing cavitation was not carried out for these two stations.

5.3 Boundary Layer Parameters on the Plate

5.3.1 Boundary Layer Thickness. The boundary layer thickness was defined to be the distance from the wall where the mean local

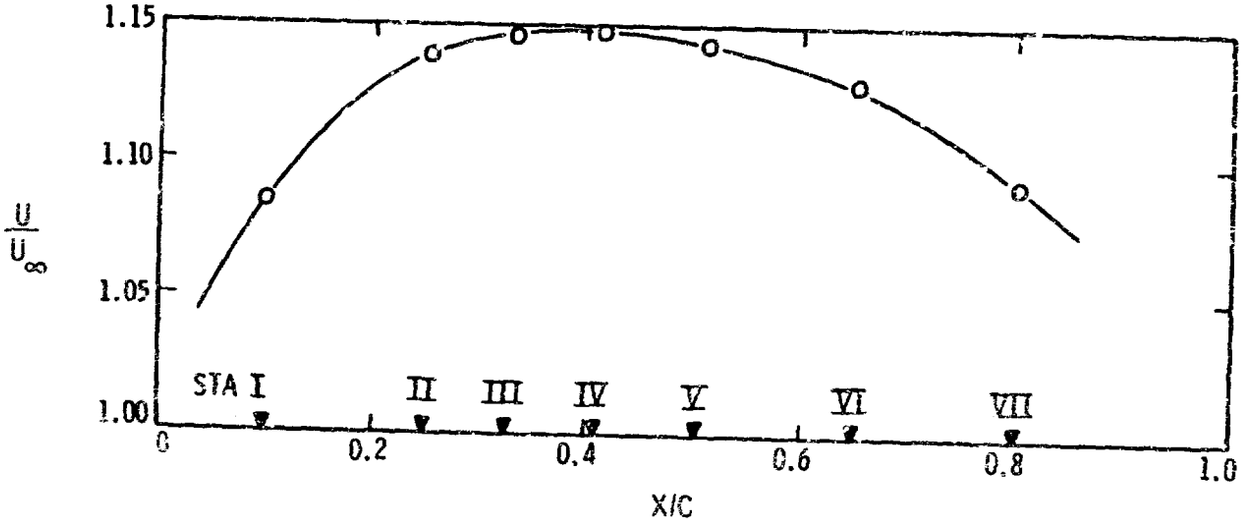

Figure 5-2. Velocity at the Edge of the Boundary Layer in the Test Section.

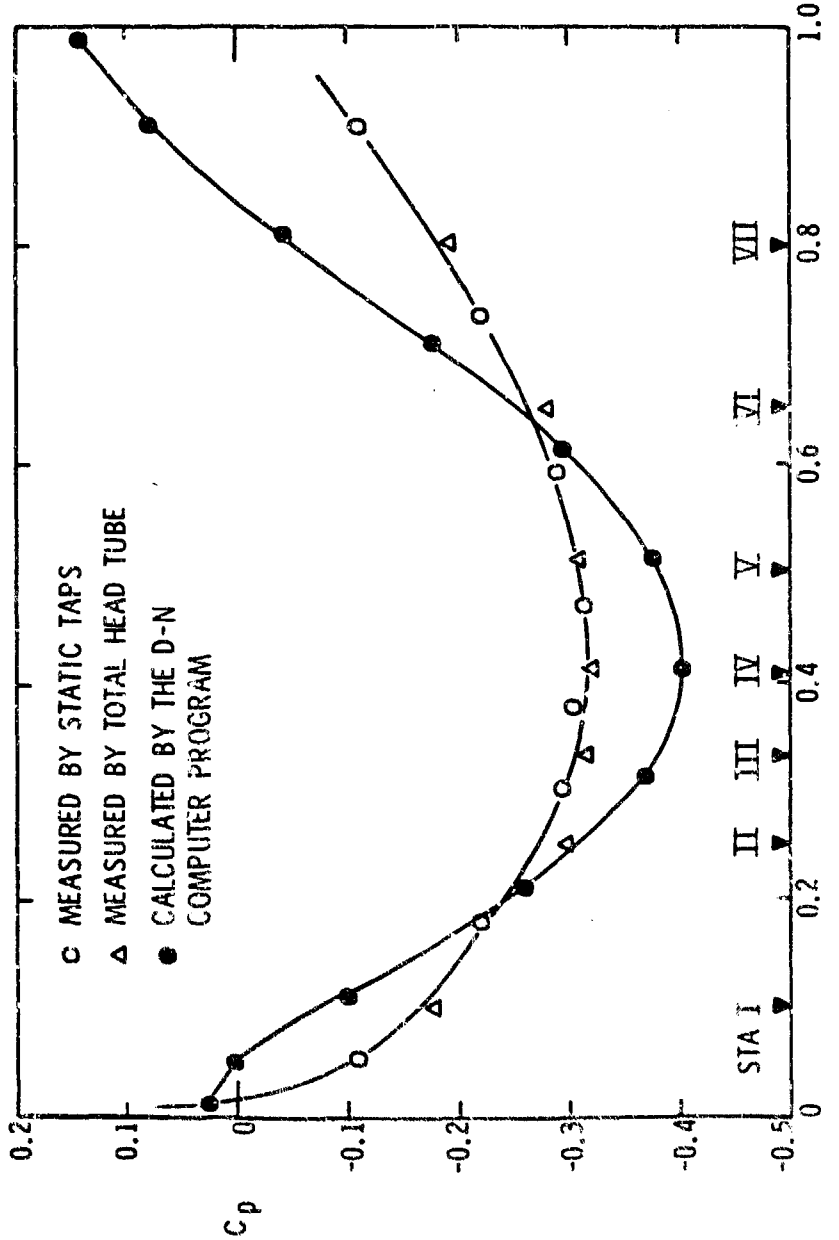

Figure 5-3. Pressure Coefficient in the Test Section.

TABLE 5-2

PRESSURE COEFFICIENTS OBTAINED BY USING STATIC TAPS

STA. NO.	1	2	3	4	5	6	7	8
$\frac{x}{c}$	0.053	0.182	0.300	0.376	0.471	0.588	0.735	0.912
Nominal Velocity (fps)								
20	0.115	0.223	0.296	0.312	0.322	0.299	0.232	0.120
30	0.116	0.219	0.295	0.306	0.313	0.287	0.221	0.111
40	0.115	0.216	0.292	0.303	0.313	0.285	0.220	0.113
50	0.117	0.218	0.290	0.303	0.310	0.286	0.218	0.112
60	0.122	0.226	0.295	0.308	0.319	0.292	0.222	0.114
Average	0.117	0.220	0.294	0.306	0.315	0.290	0.223	0.116
Standard Deviation	0.003	0.004	0.002	0.003	0.004	0.005	0.005	0.006

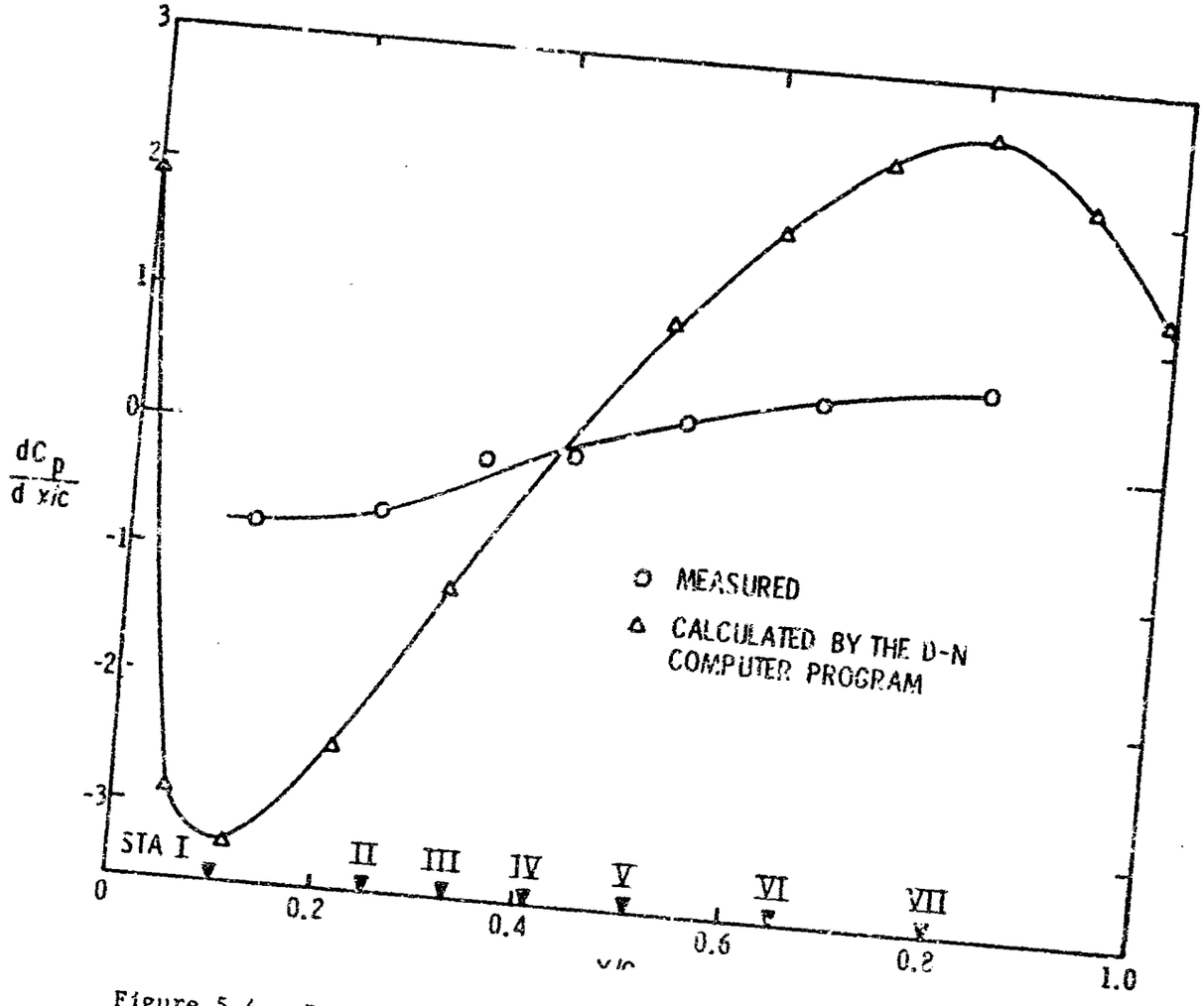

Figure 5-4. Pressure Gradient in the Test Section.

velocity is 99% of the velocity at the edge of the boundary layer. The boundary layer thickness (δ) for each station was obtained from the velocity profiles. Furthermore, these values were corrected with respect to the velocity at infinity (U_∞) equal to 40 fps at a temperature of 74^oF.

The equation used for the correction is

$$\delta = \frac{0.37x}{(Ux/\nu)^{1/5}} \tag{5-8}$$

which describes the growth of a turbulent boundary layer thickness on a flat plate. The corrected values are shown in Table 5-3 and Fig. 5-5.

5.3.2 Momentum Thickness. Other parameters such as the displacement thickness (δ^*) and the momentum thickness (θ) are given by

$$\delta^* = \int_o^\delta (1 - \frac{\bar{u}}{U}) \, dy \tag{5-9}$$

and

$$\theta = \int_o^\delta (1 - \frac{\bar{u}}{U})(\frac{\bar{u}}{U}) \, dy \, , \tag{5-10}$$

respectively, and these could not be obtained from the velocity profiles. The minimum ratios between the mean velocity ($\bar{u}$) and the velocity at the edge of boundary layer should at least be less than 0.6 for this experiment in order to obtain the momentum thickness (θ) and the displacement thickness (δ^*). Unfortunately, the minimum values obtained by the experiment are more than 0.8. To circumvent this problem, the method of E. Truckenbrodt was employed to obtain the momentum thickness (θ) and the displacement thickness (δ^*). In so doing,

TABLE 5-3

BOUNDARY LAYER THICKNESS AT EACH STATION

STA	x (inches)	U (fps)	Temp. (^{o}F)	δ^{+} (inches)	δ^{++} at U_{∞}=40fps T=74^{o}F (inches)
I	1.7	43.07	76.5	0.125	0.124
II	4.3	45.22	69.5	0.154	0.156
III	5.6	42.91	75.0	0.160	0.162
IV	7.0	42.60	74.0	0.165	0.167
V	8.7	42.52	74.0	0.180	0.183
VI	11.1	41.89	74.0	0.230	0.233
VII	13.6	40.84	75.0	0.370	0.374

+ δ as measured for each U.

++ δ at U_{∞}=40fps, T=74^{o}F was obtained by using equation (5-8) and Fig. 5-2 with respect to the velocity at infinity (U_{∞}) equal to 40 fps at the temperature of 74^{o}F.

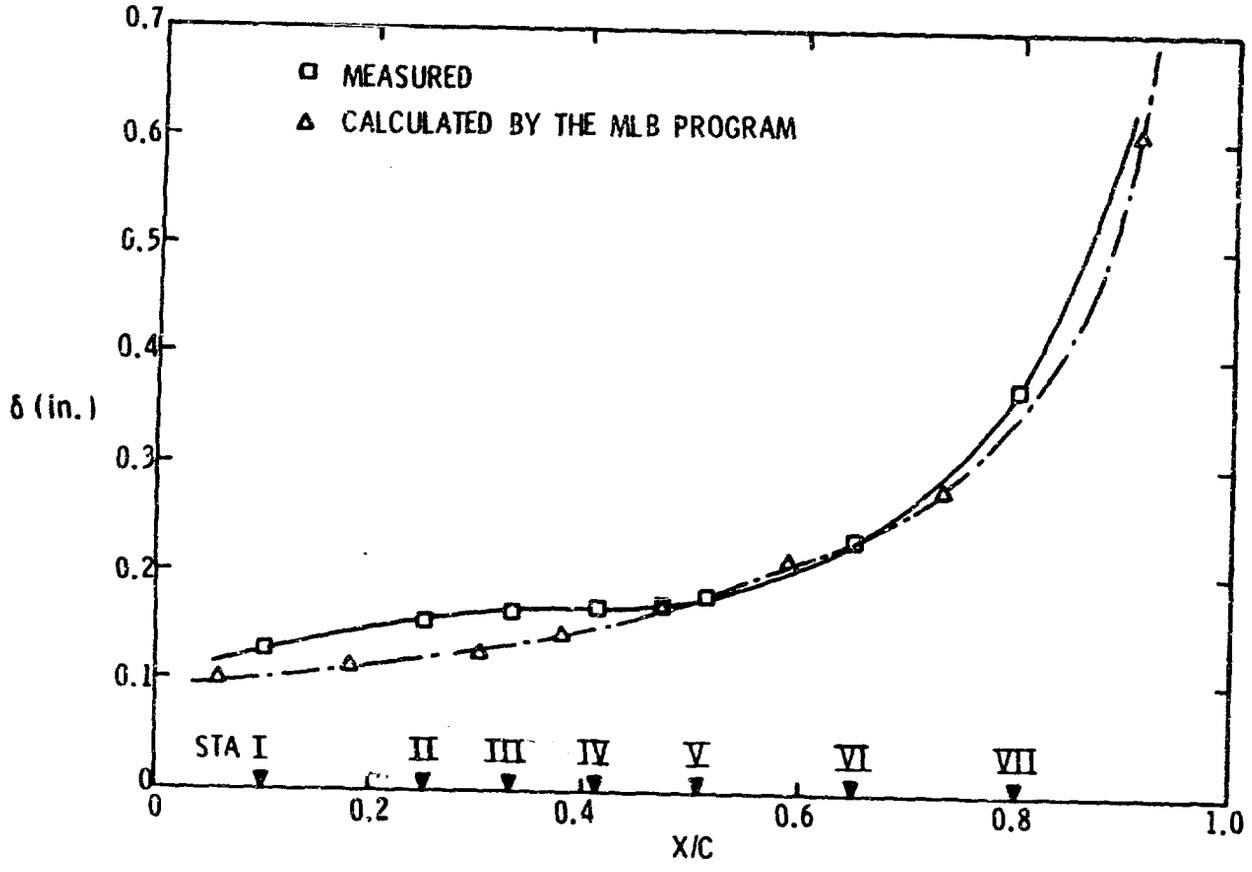

Figure 5-5. Boundary Layer Thickness in the Test Section.

two computer programs based on the method of E. Truckenbrode [35] were used. One is the MLB program which was used mainly for calculating the above parameters, and the other is an auxiliary for the MLB program, the RJD program.

First of all, the MLB computer program was used to calculate the momentum thickness (θ) and the boundary layer thickness (δ). The origin of the boundary layer was shifted back and forth in order to obtain the best agreement between calculated and experimental values of the boundary layer thickness. After these adjustments, the best agreement between calculated and measured values of the boundary layer thickness was obtained when the origin for the calculated values was one half chord length upstream of the leading edge of the curved wall, as shown in Fig. 5-5. Then the momentum thickness (δ) was calculated for the boundary layer thickness employing the origin established by the above method.

5.3.3 Shape Factors. Since the displacement thickness (δ^*) could not be obtained by the MLB computer program, the RJD computer program was used to calculate the displacement thickness and shape factor (H). By knowing the pressure distribution, the momentum thickness and a new shape factor (L) can be calculated by using the RJD computer program. The shape factor (L) is expressed in the form

$$L = \int \frac{d\bar{H}}{(H - 1)\bar{H}} , \tag{5-11}$$

where

$$H = \frac{\delta^{**}}{\theta} \; ;$$

and the energy thickness is given by

$$\delta^{**} = \int_{o}^{\delta} \left(1 - \frac{\overline{u}^2}{U^2}\right) \frac{\overline{u}}{U} \, dy \quad . \tag{5-12}$$

Initially, the momentum thickness was calculated for the origin established for the boundary layer thickness. As can be seen from Fig. 5-6, the difference between the momentum thickness calculated by the two computer programs is not insignificant. This is due to the fact that the MLB program utilizes a somewhat different skin friction coefficient (C_f) than that employed in the RJD program which is based on C_f used by Truckenbrodt. However, the calculation of the shape factor (H) via the determination of the other shape factor (L) shown in Fig. 5-7 was not sensitive to these differences in the momentum thickness (θ) as evidenced by the nearly equal values of H tabulated in Table 5-4. This lack of sensitivity to variations in H may be due to the fact that the slope of θ versus X shown in Fig. 5-6 is nearly the same for both methods of calculation.

It is felt that the determination of δ^* and θ employing the method of E. Truckenbrodt as described above is fairly accurate since it is based upon an origin determined by the experimental values of δ as described in Section 5.3.2 (see Table 5-5).

5.3.4 Shear Stress at the Wall. The experimental values for the shear stress at the wall (τ_w) can be approximated by the empirical formula

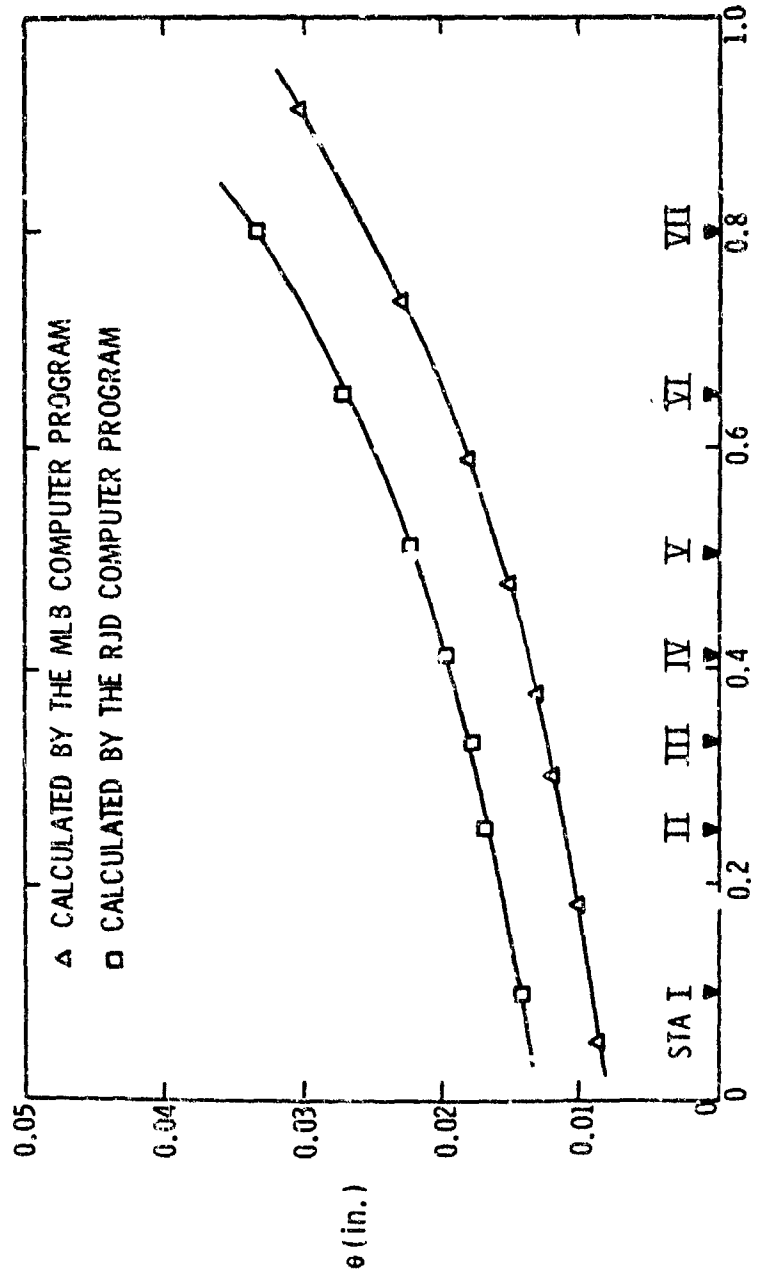

Figure 5-6. Momentum Thickness in the Test Section.

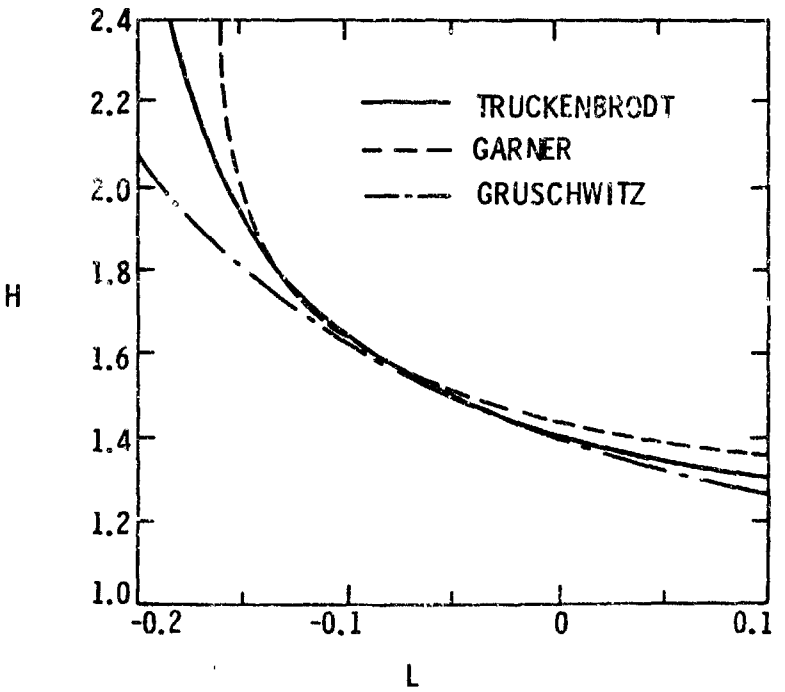

Figure 5-7. Relation Between the Shape Factors (H) and (L) for Turbulent Flow.

TABLE 5-4

PROCESS OF CALCULATIONS FOR THE BOUNDARY LAYER PARAMETERS

STA.	δ (inches) Obtained by Experiment*	δ (inches) Calculated by MLB	θ (inches) Calculated by MLB	θ (inches) Calculated by RJD	L Calculated by MLB	L Calculated by RJD	H Calculated by MLB**	H Calculated by RJD
I	0.124	0.100	0.0091	0.0142	0.0456	0.0513	1.34	1.34
II	0.156	0.119	0.0111	0.0167	0.0542	0.0636	1.33	1.33
III	0.162	0.132	0.0123	0.0176	0.0558	0.0659	1.32	1.325
IV	0.167	0.152	0.0137	0.0197	0.0478	0.0587	1.335	1.335
V	0.183	0.183	0.0159	0.0222	0.0467	0.0521	1.34	1.34
VI	0.233	0.233	0.0197	0.0270	0.0237	0.0360	1.37	1.365
VII	0.374	0.353	0.0255	0.0334	0.0190	0.0177	1.39	1.390
Figure	Fig. 5-5		Fig. 5-6		-----		-----	

---

* The measured values of δ were used to determine h/δ in the $\sigma_{\ell fp}$ correlation (Section 5.4.4) and were corrected for various velocities in accordance with the procedure outlined in Table 5-3.

** These values were used to calculate δ^*, τ_w and β.

TABLE 5-5

BOUNDARY LAYER PARAMETERS AT EACH STATION *

STA	$\frac{x}{c}$	δ (inches)	δ^* (inches)	θ (inches)	H
I	0.10	0.124	0.0122	0.0091	1.34
II	0.25	0.156	0.0148	0.0111	1.33
III	0.33	0.162	0.0162	0.0123	1.32
IV	0.41	0.167	0.0183	0.0137	1.335
V	0.51	0.183	0.0213	0.0159	1.34
VI	0.65	0.233	0.0270	0.0197	1.37
VII	0.80	0.374	0.0354	0.0255	1.39

*These parameters were calculated for a velocity at infinity (U_∞) of 40 fps (see Section 5.3.1)

$$\frac{\tau_w}{\rho U^2} = 0.123 \times 10^{-0.678H} \left(\frac{U\theta}{\nu}\right)^{-0.268} \qquad (5\text{-}13)$$

which was given by Ludwieg-Tillman [36]. The shear stress at the wall was calculated by substituting the boundary layer parameters which were obtained in Section 5.3.2 and 5.3.3 into equation (5-13). Furthermore, Clauser's equilibrium parameter (β), the shape factor (G) and the wake parameter (Π) were calculated from equations (2-14), (2-18) and (2-22), respectively, and are tabulated in Table 5-6 and Table 5-7.

5.4 Cavitation Number

5.4.1 Cavitation Number for the Case of Zero Pressure Gradient.

The cavitation number ($\sigma_{\ell fp}$) for the case of zero pressure gradient was measured at STA. IV, and is tabulated in Table 5-8. The effect of the relative height (h/δ) has been known to be the most dominant factor for this case and the relationship between the cavitation number ($\sigma_{\ell fp}$) and the relative height for this investigation (h/δ) is shown by the experimental data in Fig. 5-8. A comparison of the present result with that of Ref. [29] was carried out and is shown in Fig. 5-9. For these two investigations, Fig. 5-8 and Fig. 5-9 show that the relationship between the log of the cavitation number and the log of the relative height is linear. By neglecting the effect of Reynold's number, these relationships can be expressed in the form

$$\sigma_{\ell fp} = \text{constant} \left(\frac{h}{\delta}\right)^a . \qquad (5\text{-}14)$$

TABLE 5-6

WALL SHEAR STRESS AT EACH STATION

STA	$\frac{x}{c}$	U (ft/sec)	θ (inches)	H	τ_w* (lb/ft^2)
I	0.10	43.30	0.0091	1.34	3.366
II	0.25	45.31	0.0111	1.33	3.508
III	0.33	45.83	0.0123	1.32	3.537
IV	0.41	46.04	0.0137	1.335	3.381
V	0.51	45.92	0.0159	1.34	3.209
VI	0.65	45.17	0.0197	1.37	2.811
VII	0.80	43.69	0.0255	1.39	2.401

* These values were calculated by using equation (5-13) (see Section 5.3.4).

TABLE 5-7

SHAPE FACTOR (G) AND WAKE PARAMETER (Π) AT EACH STATION

STA	$\frac{x}{c}$	δ^* (inches)	τ_w (lb/ft^2)	dp/dx_3 (lb/ft^3)	β	Π	G
I	0.10	0.0122	3.356	-584.2	-0.176	0.344	6.100
II	0.25	0.0148	3.508	-438.2	-0.154	0.361	6.150
III	0.33	0.0162	3.537	-219.1	-0.084	0.414	6.314
IV	0.41	0.0183	3.381	- 58.4	-0.026	0.457	6.448
V	0.51	0.0213	3.209	+145.1	+0.081	0.532	6.688
VI	0.65	0.0270	2.811	+321.3	+0.257	0.649	7.070
VII	0.80	0.0354	2.401	+438.2	+0.538	0.823	7.647

The shape factor (G), wake parameter (Π) and Clauser's equilibrium parameter (β) were calculated by using equations (2-18), (2-22) and (2-14), respectively.

TABLE 5-8

LIMITED CAVITATION DATA STA. IV ($\frac{dp}{dx} \simeq 0$)

$\frac{h}{\delta}$	U_∞ (fps)	U (fps)	Gas Content (ppm)	Water Temp. (^oF)	$\sigma_{\ell fp}$*	Standard Deviation of $\sigma_{\ell fp}$
0.058	29.77	34.27	2.90		0.270	0.004
0.060	38.82	44.69	to	68.0	0.292	0.017
0.063	60.36	69.48	3.28		0.322	0.013
0.290	29.88	34.39	1.50		0.646	0.011
0.299	38.59	44.42	to	70.0	0.666	0.015
0.312	61.26	70.51	2.93		0.676	0.004
0.581	29.73	34.22	1.98		0.912	0.026
0.599	38.38	44.18	to	67.5	0.901	0.030
0.625	60.27	69.37	3.12		0.872	0.014
1.736	29.46	33.91	2.13		1.836	0.090
1.790	38.06	43.81	to	68.0	1.847	0.144
-	-	-	4.50		-	-

* These are mean values for seven measurements.

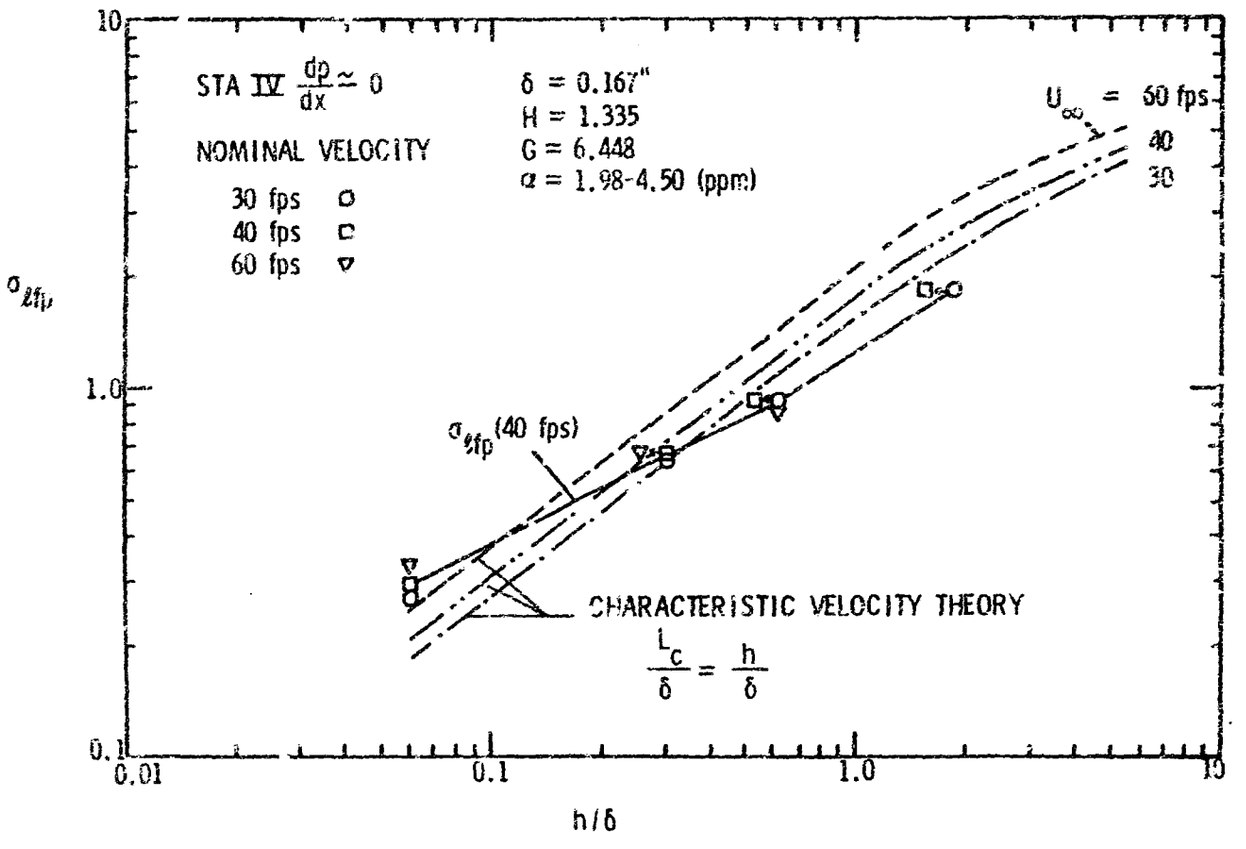

Figure 5-8. Variation of Cavitation Number with Relative Height.

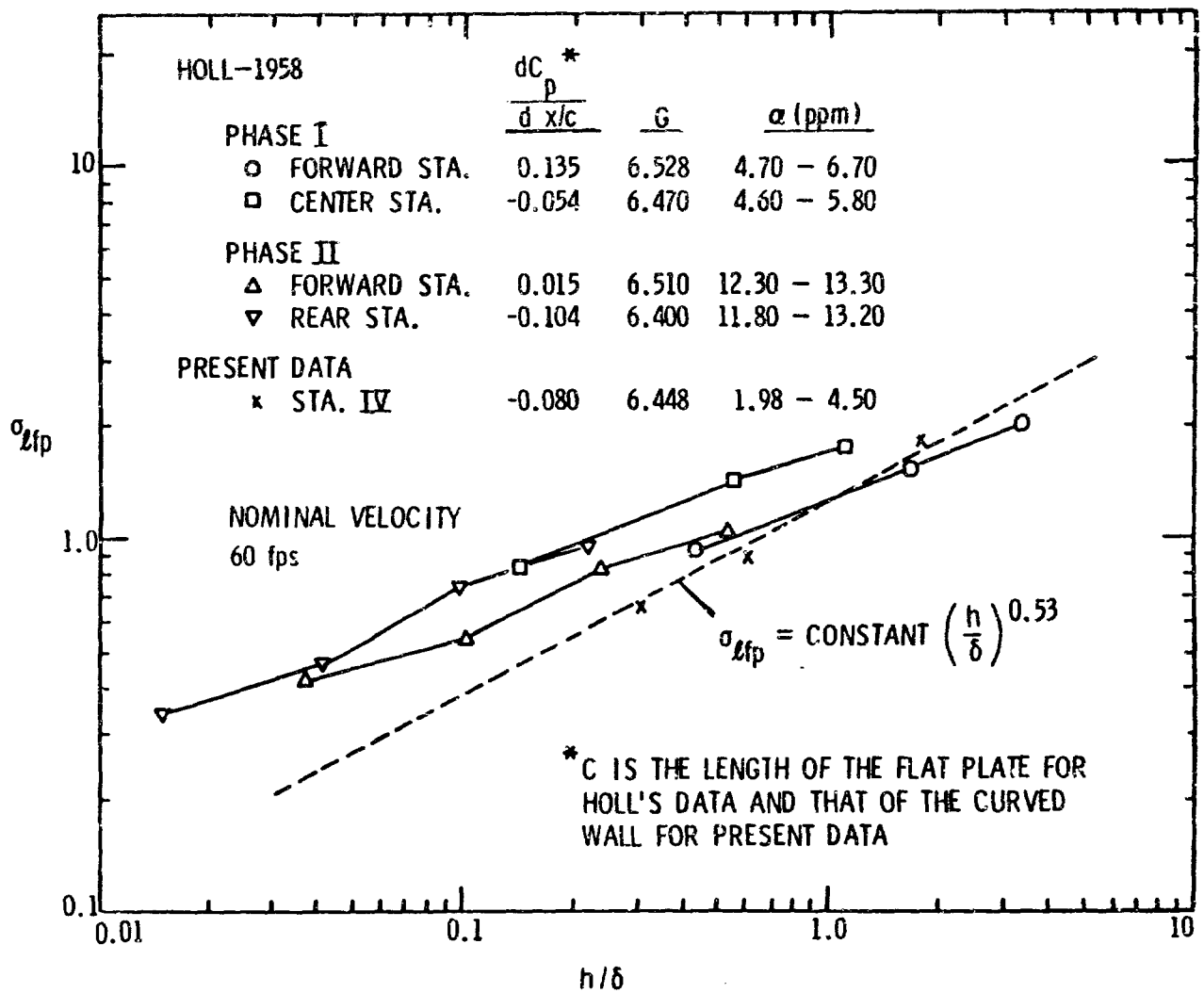

Figure 5-9. Comparison of Present $\sigma_{\ell fp}$ versus $(\frac{h}{\delta})$ with that of Ref. [29] for Zero Pressure Gradient.

The power number 'a' and the correlation coefficient (R) were calculated by using

$$a = \frac{\sum_{i=1}^{n} \log(\frac{h}{\delta})_i \log(\sigma_{\ell fp})_i - \frac{\sum_{i=1}^{n} \log(\frac{h}{\delta})_i \sum_{i=1}^{n} \log(\sigma_{\ell fp})_i}{n}}{\sum_{i=1}^{n} \left[\log(\frac{h}{\delta})\right]_i^2 - \frac{\left[\sum_{i=1}^{n} \log(\frac{h}{\delta})_i\right]^2}{n}} \tag{5-15}$$

and

$$R = \frac{a\, \sigma_{\log(\frac{h}{\delta})}}{\sigma_{\log(\sigma_{\ell fp})}} \tag{5-16}$$

where a was obtained by the least squares method, $\sigma_{\log(\frac{h}{\delta})}$ and $\sigma_{\log(\sigma_{\ell fp})}$ are standard deviations of $\log(\frac{h}{\delta})$ and $\log(\sigma_{\ell fp})$, respectively.

'a' is 0.53 for the correlation coefficient 0.9969 for the present experiment whereas 'a' has the value 0.40 for the experiment of Ref. [29]. This difference in 'a' for the two experiments may be due to gas content effects. The present experiments were carried out with the gas contents between 1.91 ppm and 5.52 ppm. On the other hand, the experiments of Ref. [29] were conducted for gas contents of 3.46 ppm to 15.66 ppm. For comparison purposes the data of Ref. [29] were corrected for different gas contents. The equation used for the correction is

$$\sigma_{R\text{-corr}} = \sigma_R - \frac{K(\alpha_R - 3.71)}{1/2\ \rho U_\infty^2} \tag{5-17}$$

where k is 0.104, σ_R is a limited cavitation number of Ref. [29], and α_R is a gas content of Ref. [29]. The derivation of equation (5-17) is demonstrated in Appendix B. The corrected cavitation numbers are shown in Fig. 5-10, which demonstrates that the slope of the variable between the log of the corrected cavitation number to the log of the relative height becomes almost the same as the present one. It might be said that 0.53 is a more universal value for a specific gas content, i.e., α = 3.71 ppm than the value of 0.40 employed in Ref. [33]. Thus

$$\sigma_{\ell fp} = \text{constant } (\frac{h}{\delta})^{0.53} \quad . \tag{5-18}$$

However, the effect of Reynold's number based on boundary layer thickness should be accounted for to obtain a more accurate relationship. This will be discussed in Section 5.4.3.

5.4.2 Effect of Pressure Gradient on Cavitation. The cavitation numbers for the case of favorable and unfavorable pressure gradient were measured at STA. I and STA. VII and are tabulated in Tables 5-9 and 5-10, respectively. Fig. 5-11 shows that the relationships between the log of the cavitation number and the log of the relative height are almost linear. The slopes are 0.576 for the correlation coefficient (R) of 0.9885 for the case of a favorable pressure gradient, and 0.481 for R equal to 0.9882 for the case of an unfavorable pressure gradient. The cavitation data for zero pressure gradient lies in between the data shown in Fig. 5-11 and never exceeds those for the case of unfavorable pressure gradient. In other words, the cavitation numbers tend to increase with the pressure gradient.

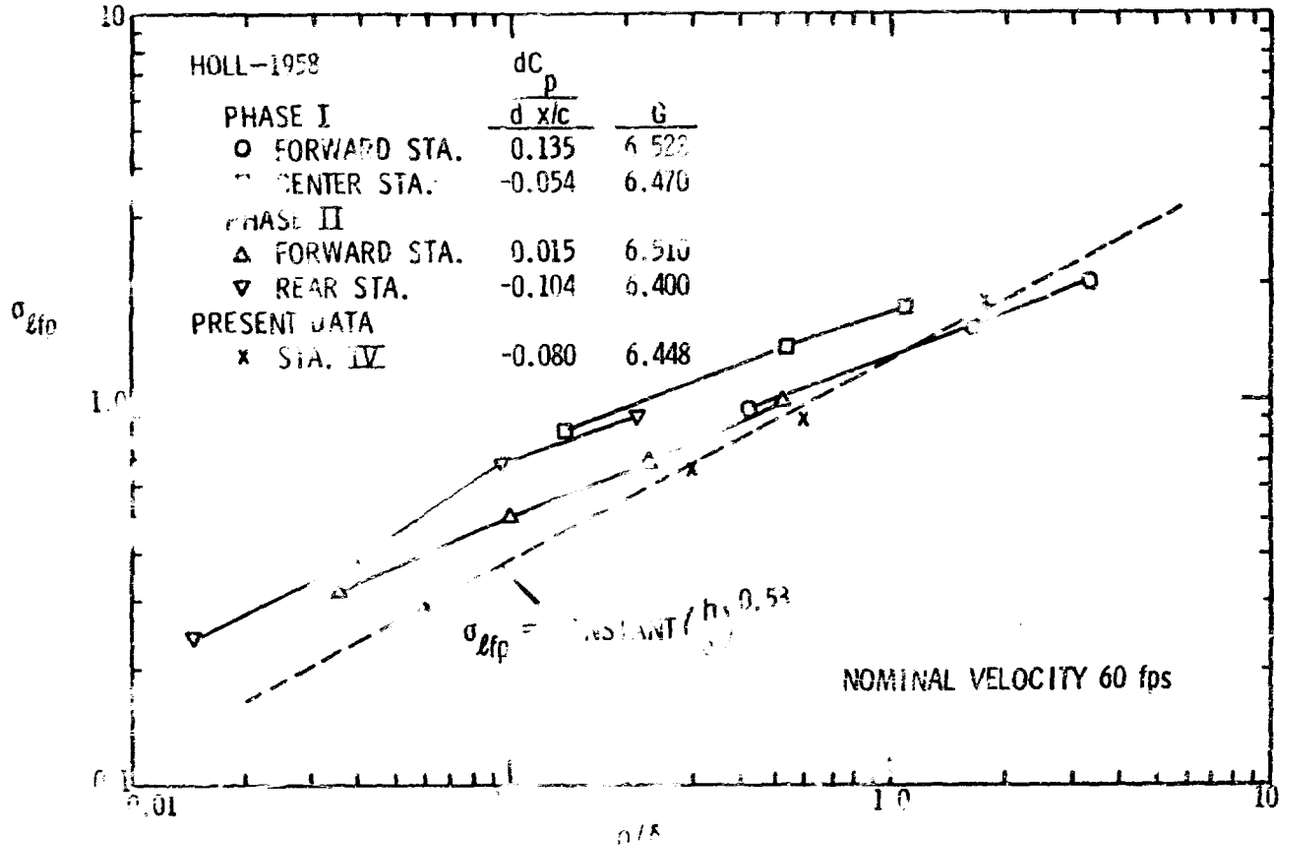

Figure 5-10. Comparison of Present [illegible] versus $(\frac{h}{\delta})$ with that of Ref. [29]. Corrected to α of 3.7 ppm.

TABLE 5-9

LIMITED CAVITATION DATA, STA. I ($\frac{dp}{dx} < 0$)

$\frac{h}{\delta}$	U_∞ (fps)	U (fps)	Gas Content (ppm)	Water Temp. (°F)	$\sigma_{\ell fp}$*	Standard Deviation of $\sigma_{\ell fp}$
0.079	30.07	35.58	2.60		0.247	0.016
0.081	38.82	42.07	to	68.0	0.265	0.006
0.085	60.89	65.98	3.90		0.310	0.005
0.156	29.60	32.07	2.91		0.503	0.010
0.161	37.49	40.62	to	67.0	0.545	0.002
0.168	59.39	64.35	4.05		0.603	0.006
0.548	29.31	31.76	1.98		0.886	0.017
0.565	37.89	41.06	to	68.5	0.886	0.006
0.590	59.01	63.88	2.72		0.946	0.007
0.782	29.63	32.10	3.85		1.040	0.014
0.806	38.31	41.51	to	69.5	1.065	0.013
0.841	59.32	64.27	4.50		1.107	0.025
2.347	29.41	31.87	2.52		2.130	0.061
2.420	37.79	40.95	to	71.5	2.125	0.053
2.526	47.98	51.99	3.52		2.470	0.056

* These are mean values for seven measurements.

TABLE 5-10

LIMITED CAVITATION DATA, STA. VII ($\frac{dp}{dx} > 0$)

$\frac{h}{\delta}$	U_∞ (fps)	U (fps)	Gas Content (ppm)	Water Temp. (^oF)	$\sigma_{\ell fp}$*	Standard Deviation of $\sigma_{\ell fp}$
0.026	38.77	42.35	2.25		0.268	0.006
0.027	49.30	53.84	to	71.0	0.281	0.001
0.028	60.83	66.44	3.15		0.281	0.009
0.051	30.07	32.84	3.30		0.465	0.008
0.052	38.82	42.40	to	66.0	0.506	0.003
0.055	61.10	66.74	5.21		0.477	0.010
0.180	29.82	32.57	3.98		0.750	0.011
0.186	37.85	41.34	to	72.0	0.787	0.010
0.194	59.92	65.45	5.52		0.851	0.005
0.389	30.01	32.78	3.15		1.012	0.030
0.401	38.87	42.45	to	70.0	0.985	0.012
-	-	-	5.32		-	-
0.778	29.46	32.18	2.36		1.612	0.082
0.802	37.89	41.38	to	70.0	1.580	0.035
0.837	48.36	52.82	3.81		1.697	0.020

* These are mean values for seven measurements.

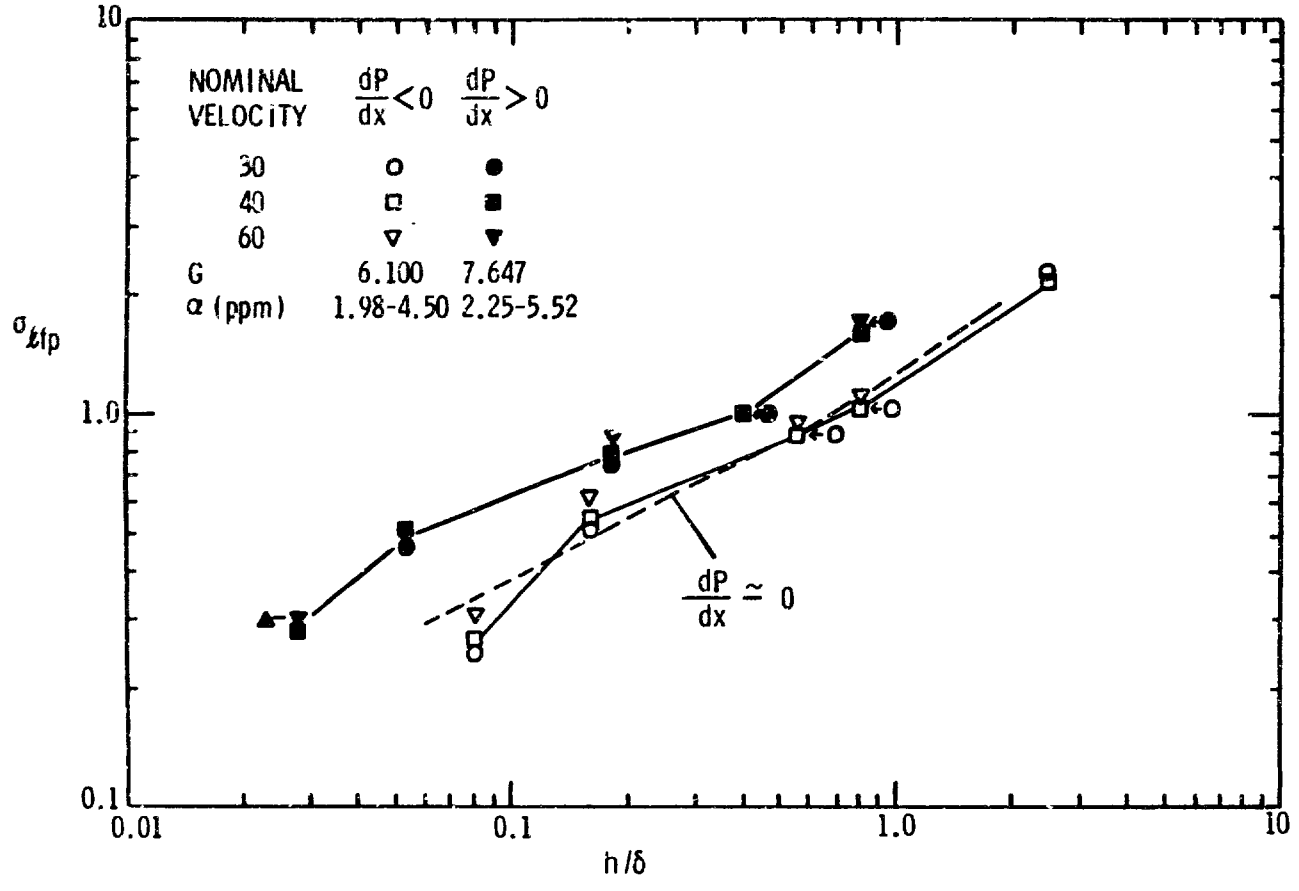

Figure 5-11. Variation of Cavitation Number with Relative Height for Finite Pressure Gradients.

According to equation (3-7) used in the characteristic velocity theory, that is,

$$\sigma_{\ell fp} = \left(\frac{u_c}{U}\right)^2 \sigma_{\ell fp}' \qquad (3\text{-}7)$$

the velocity profile for a favorable pressure gradient, as shown in Fig. 2-1, must promote the onset of cavitation. However, this investigation showed that the cavitation number increased with the pressure gradient, which is in contradiction with the characteristic velocity theory. This discrepancy may be due to the complicated flow, i.e., separated flow, caused by the triangular protrusion.

As discussed in Section 2.3, the shape factors (H) and (G), and wake parameter (Π) can be considered as factors to be related to pressure gradient. In order to obtain the most consistent relationship between cavitation number and one of these three factors, the calculation was done by using the present data and did not include the data of Holl [29]. Fig. 5-12 shows that power-law correlations of $\sigma_{\ell fp}$ with G and Π could be obtained for the present data. The correlation coefficient for each h/δ and the average percent error in slope are 0.993 and 18.0%, respectively, for correlation of $\sigma_{\ell fp}$ with G and 0.9901 and 21.4% for that of $\sigma_{\ell fp}$ with Π. It is seen that the correlation of $\sigma_{\ell fp}$ with G is more consistent than that of Π. However, Π may be an alternative parameter to G whereas the parameter H may be primarily limited to the case dp/dx = 0.

Thus, the relationship between the cavitation number ($\sigma_{\ell fp}$) and the shape factor (G) is expressed for the same relative height and Reynold's number in the form

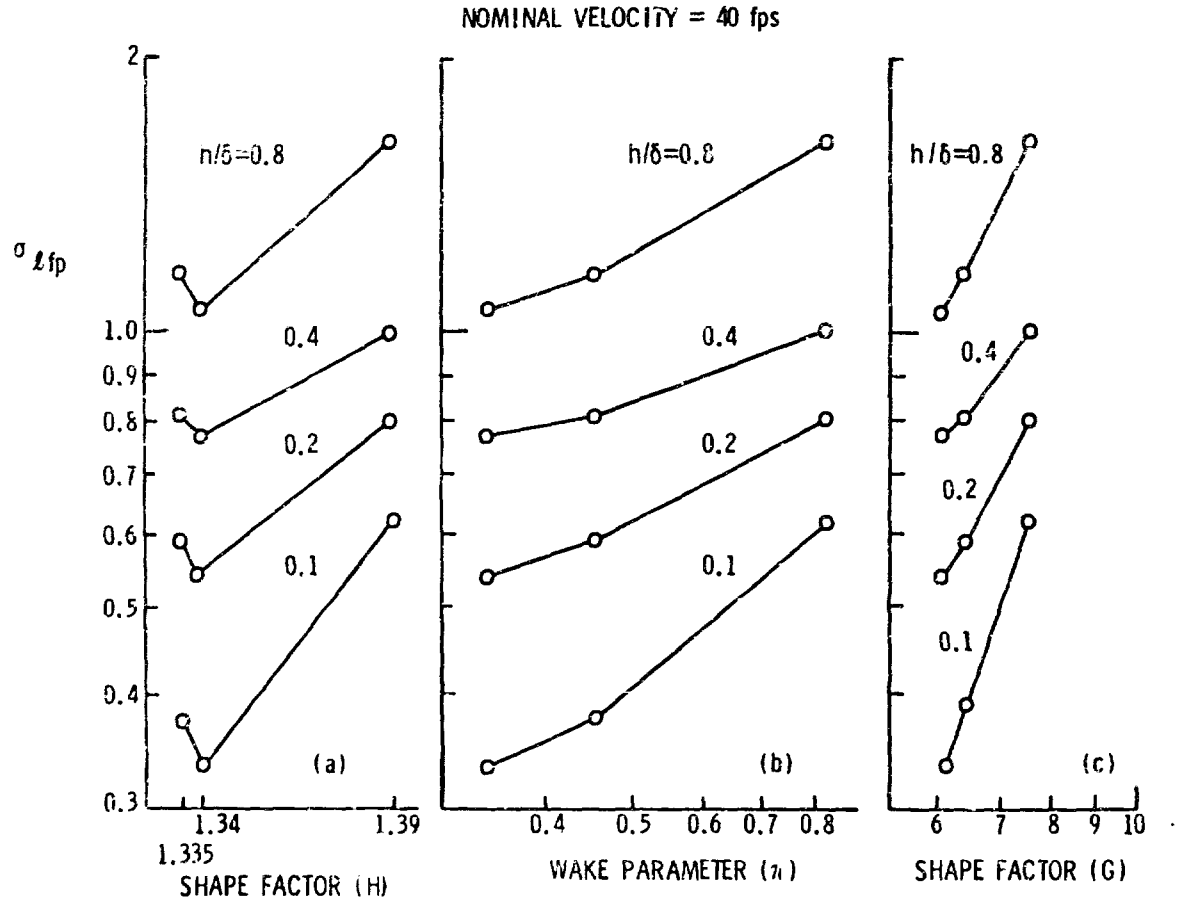

Figure 5-12. Variation of Cavitation Number with H, Π and G.

$$\sigma_{\ell fp} = \text{constant } (G)^{1.25} \quad . \tag{5-19}$$

5.4.3 Effect of Reynold's Number on Cavitation. As indicated in Section 3.5, Reynold's number based on the boundary layer thickness is an important parameter. However, the influence of Reynold's number is less dominant than the relative height or the shape factor (G), as shown in Figs. 5-8 and 5-11. The relationship between the cavitation number and the Reynold's number for constant relative height and shape factor (G) has the form

$$\sigma_{\ell fp} = \text{constant } \left(\frac{U\delta}{\nu}\right)^{0.194} \quad . \tag{5-20}$$

Since the exponent 0.194 is close to the value 0.20 determined by Arndt et al. [33], the value 0 20 was used throughout this analysis. Hence

$$\sigma_{\ell fp} = \text{constant } \left(\frac{U\delta}{\nu}\right)^{0.20} \quad . \tag{5-21}$$

5.4.4 The Cavitation Law for Two Dimensional Triangular Protrusions.

The cavitation law for a two dimensional triangular protrusion can be expressed in the form

$$\sigma_{\ell fp} = C\left(\frac{h}{\delta}\right)^{0.53} \left(\frac{U\delta}{\nu}\right)^{0.2} (G)^{1.25} \quad . \tag{5-22}$$

When applied to the data from this investigation the above correlation gives a good estimate of the cavitation number with an average error of 10.3% with respect to the measured values. The equation is compared with experimental data in Fig. 5-13.

	h/δ	$U_\infty \delta/\nu$	G
● $\frac{dP}{dx} \simeq 0$	0.058–1.790	43,400–86,800	6.448
△ $\frac{dP}{dx} < 0$	0.070–2.526	32,200–64,400	6.100
▲ $\frac{dP}{dx} > 0$	0.026–0.837	97,200–194,400	7.647

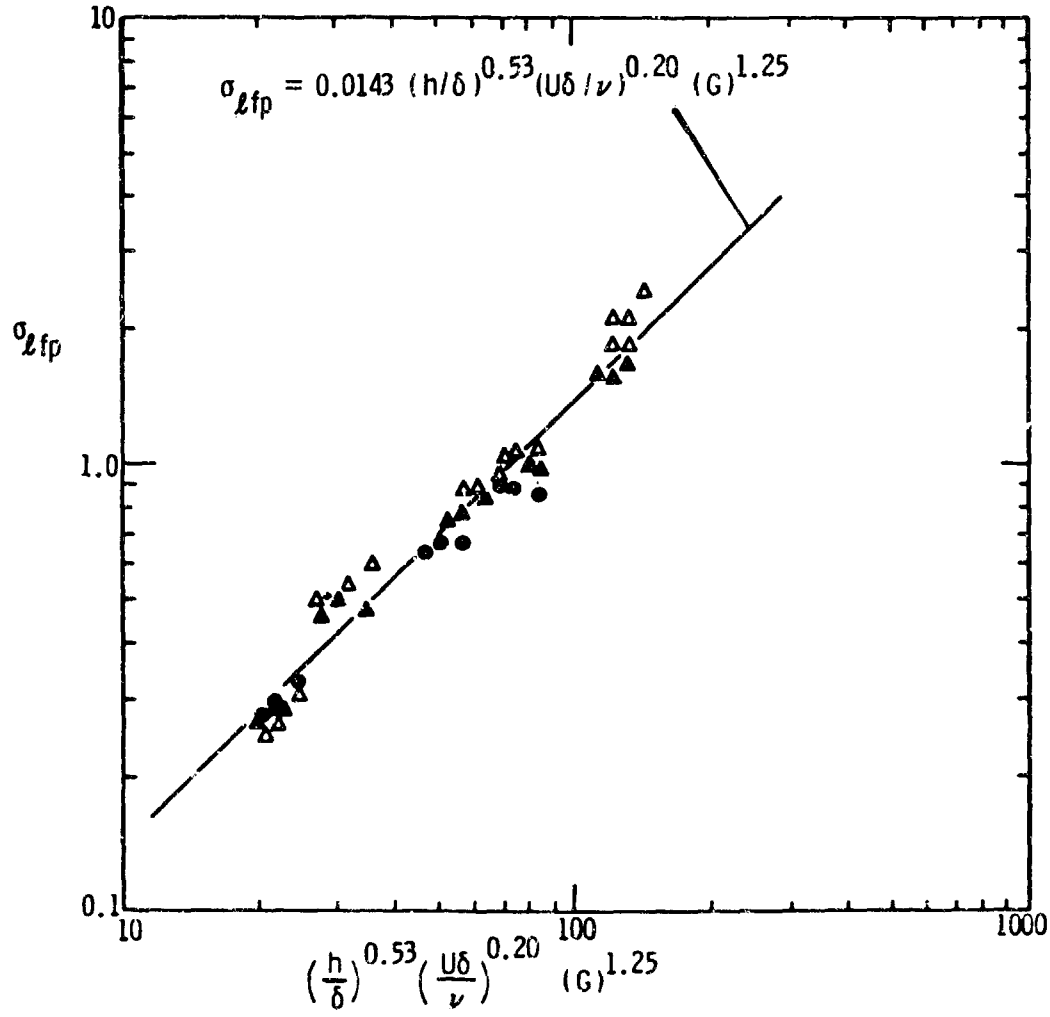

Figure 5-13. Cavitation Law for Isolated Roughness - (Present Investigation).

As shown in Fig. 5-14, a fair agreement was obtained with the results of Holl for $\frac{dp}{dx} = 0$, when corrected to a gas content of 3.71 ppm as described in Appendix B.

5.5 Development of the Characteristic Velocity Theory

As discussed in Section 3.4, $\sigma_{\ell fp}$ is expressed as

$$\sigma_{\ell fp} = \frac{1}{H} \left(\frac{h}{\delta}\right)^{\frac{2}{m}} \sigma'_{\ell fp} \quad \text{for} \quad \frac{h}{\delta} \leq 1 \tag{3-10}$$

and

$$\sigma_{\ell fp} = 1 - \frac{\delta}{h} \left(1 - \frac{1}{H}\right) \sigma'_{\ell fp} \quad \text{for} \quad \frac{h}{\delta} \geq 1 \tag{3-11}$$

where $\sigma'_{\ell fp}$ is the limited cavitation number for the roughness in the absence of a boundary layer, that is, $h/\delta = \infty$. For the two dimensional triangular roughness, $\sigma'_{\ell fp}$ was assumed to be equal to that of a sharp-edged flat plate obtained by J. W. Holl and C. B. Baker of the Applied Research Laboratory at The Pennsylvania State University, and is shown in Fig. 5-15. By the method of least squares, $\sigma'_{\ell pf}$ was calculated to be

$$\sigma'_{\ell fp} = 0.0214 \ Re_h^{0.424} \tag{5-23}$$

where Re_h is the Reynold's number based on the height of the roughness.

Examples of the application of this theory based on equation (5-23) are shown in Fig. 5-8 for the nominal velocities 40, 50 and 60 fps. As shown in Fig. 5-8, it is seen that $\sigma_{\ell fp}$ calculated by the characteristic velocity theory is in fair agreement with the experimental data for $0.06 < h/\delta \leq 1.79$, which was the investigated

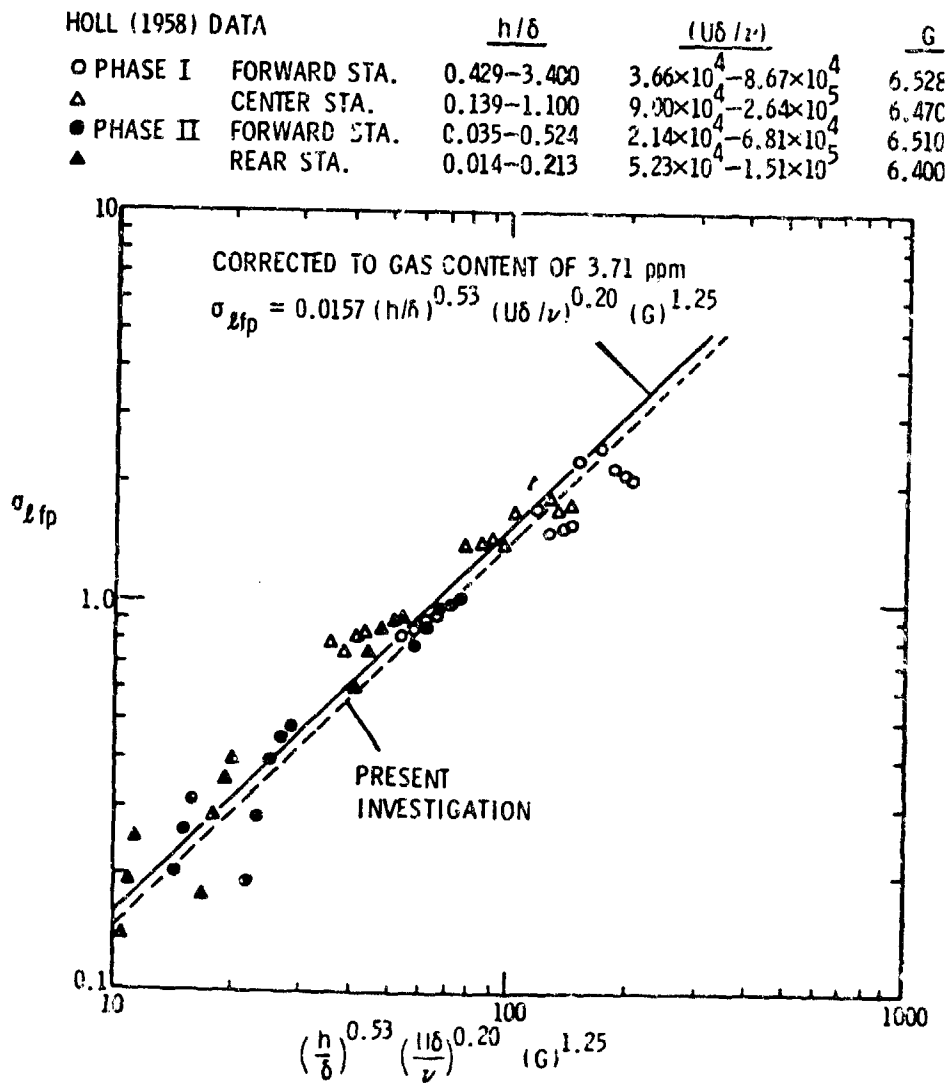

Figure 5-14. Cavitation Law for Isolated Roughness - (Comparison of Present Investigation and Holl - 1958).

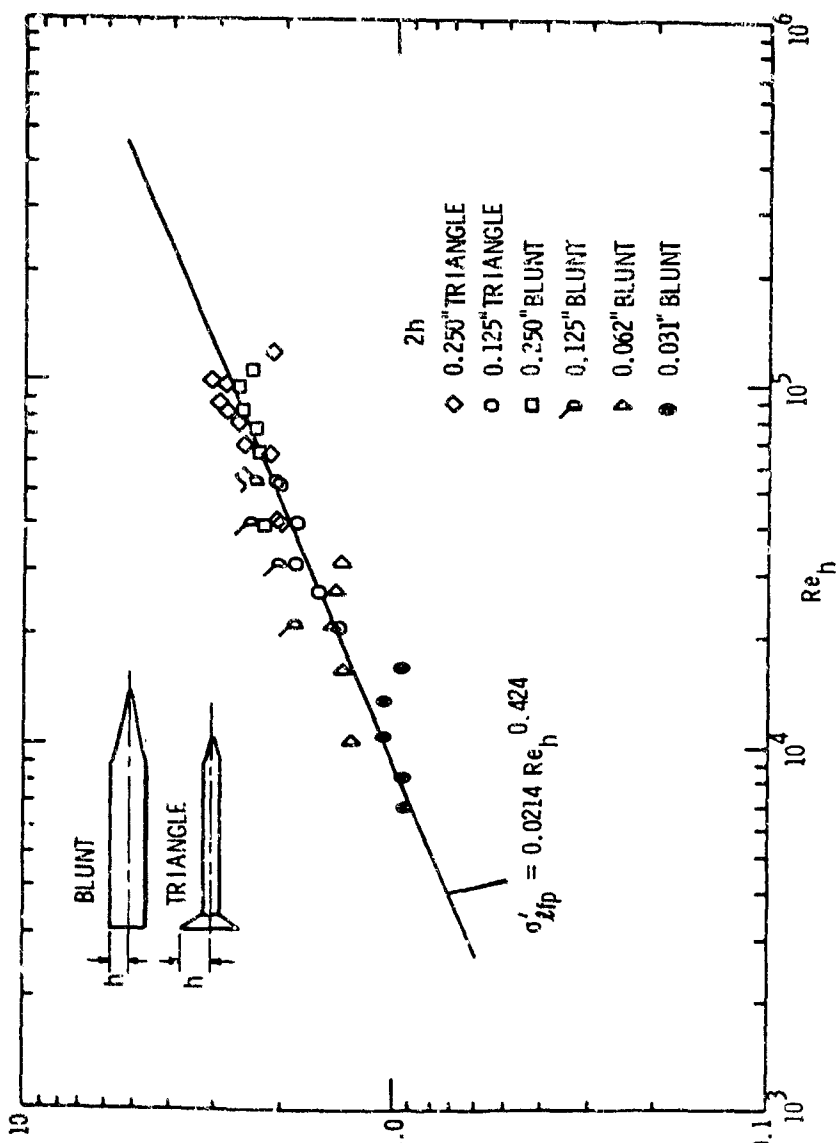

Figure 5-15. Cavitation Number versus Re_h for Sharp-Edged Flat Plates in a Uniform Stream.

region. However, significant differences may occur for cases outside the scope of the present investigation.

As mentioned in Section 3.4, Holl [4] assumed that the characteristic length (L_c) is closely related to the height of the irregularity (h). Thus, it was assumed that L_c is equal to h. However, one of the main reasons for the discrepancy between the result calculated by the characteristic velocity theory and the experimental data may be due to the above assumption. Therefore, h in equation (3-10) should be changed to L_c as

$$\sigma_{\ell fp} = \frac{1}{H} \left(\frac{L_c}{\delta}\right)^{\frac{2}{m}} \sigma'_{\ell fp} \quad \text{for} \quad \frac{L_c}{\delta} \leq 1 \tag{5-24}$$

and

$$\sigma_{\ell fp} = 1 - \frac{\delta}{L_c} \left(1 - \frac{1}{H}\right) \sigma'_{\ell fp} \quad \text{for} \quad \frac{L_c}{\delta} \geq 1 \quad . \tag{5-25}$$

Furthermore, L_c was derived semi-empirically so that good agreement between the two results could be obtained.

Employing equation (3-7) for the experimental value of $\sigma_{\ell fp}$ ($\sigma_{\ell fp\text{-}exp}$) gives

$$\sigma_{\ell fp\text{-}exp} = \left(\frac{U_c}{U_\infty}\right)^2 \sigma'_{\ell fp} \quad . \tag{5-26}$$

or

$$\left(\frac{U_c}{U_\infty}\right)^2 = \frac{\sigma_{\ell fp\text{-}exp}}{\sigma'_{\ell fp}} \quad . \tag{5-27}$$

By employing equation (5-22), one can express $\sigma_{\ell fp\text{-}exp}$ in the form

$$\sigma_{\ell fp-exp} = 0.0143 \left(\frac{h}{\delta}\right)^{0.53} \left(\frac{U\delta}{\nu}\right)^{0.2} (G)^{1.25} \qquad (5\text{-}28)$$

or for a zero pressure gradient

$$\sigma_{\ell fp-exp} = 0.147 \left(\frac{h}{\delta}\right)^{0.53} \left(\frac{U_\infty \delta}{\nu}\right)^{0.2} , \qquad (5\text{-}29)$$

where G is equal to 6.447.

Substitution of equations (5-23) and (5-29) into equation (5-27) results in

$$\left(\frac{\bar{U}_c}{U_\infty}\right)^2 \simeq 7.000 \left(\frac{h}{\delta}\right)^{0.11} \left(\frac{U_\infty \delta}{\nu}\right)^{-0.2} . \qquad (5\text{-}30)$$

By knowing equation (3-7), and by substitution of equation (5-30) into equation (5-24) and equation (5-25) one gets

$$\frac{L_c}{\delta} = \left(7.00 \frac{m+2}{m}\right)^{\frac{m}{2}} \left(\frac{h}{\delta}\right)^{0.055m} \left(\frac{U_\infty \delta}{\nu}\right)^{-0.11m} \quad \text{for } \frac{L_c}{\delta} \leq 1 \qquad (5\text{-}31)$$

and

$$\frac{L_c}{\delta} = \frac{2}{m+2} \frac{1}{1 - 7.00\left(\frac{h}{\delta}\right)^{0.11} \left(\frac{U_\infty \delta}{\nu}\right)^{-0.22}} \quad \text{for } \frac{L_c}{\delta} \geq 1 \qquad (5\text{-}32)$$

Employing equation (3-12) in equations (5-31) and (5-32) results in

$$\frac{L_c}{\delta} = (7H)^{\frac{m}{2}} \left(\frac{h}{\delta}\right)^{0.055m} \left(\frac{U_\infty \delta}{\nu}\right)^{-0.11m} \quad \text{for } \frac{L_c}{\delta} \leq 1 \qquad (5\text{-}33)$$

and

$$\frac{L_c}{\delta} = \left(1 - \frac{1}{H}\right) \frac{1}{1 - 7\left(\frac{h}{\delta}\right)^{0.11} \left(\frac{U_\infty \delta}{\nu}\right)^{-0.22}} \quad \text{for } \frac{L_c}{\delta} \geq 1 \quad . \tag{5-34}$$

Equations (5-33) and (5-34) indicate that the dimensionless characteristic length (L_c/δ) for a zero pressure gradient is a function of the shape factor (H) and the Reynold's number based on the boundary layer thickness in addition to the dimensionless relative height (h/δ). Equation (5-33) is plotted in Fig. 5-16 over a range of parameters corresponding to Fig. 5-8. It is seen that in order for L_c/δ to be greater than one, h/δ would have to be significantly greater than one. Furthermore, equations (5-33) and (5-34) are plotted in Fig. 5-17. They show that the relationship between L_c/δ and h/δ is sensitive to Re_δ, especially for the case where L_c/δ is greater than one. However, since these two equations were obtained from the results of this investigation over the Re_δ range of 3×10^4 to 2×10^5 and the h/δ range of 0.06 to 2.50, care should be taken in using equations (5-33) and (5-34) for values of Re_δ and h/δ outside of the aforementioned range of these parameters.

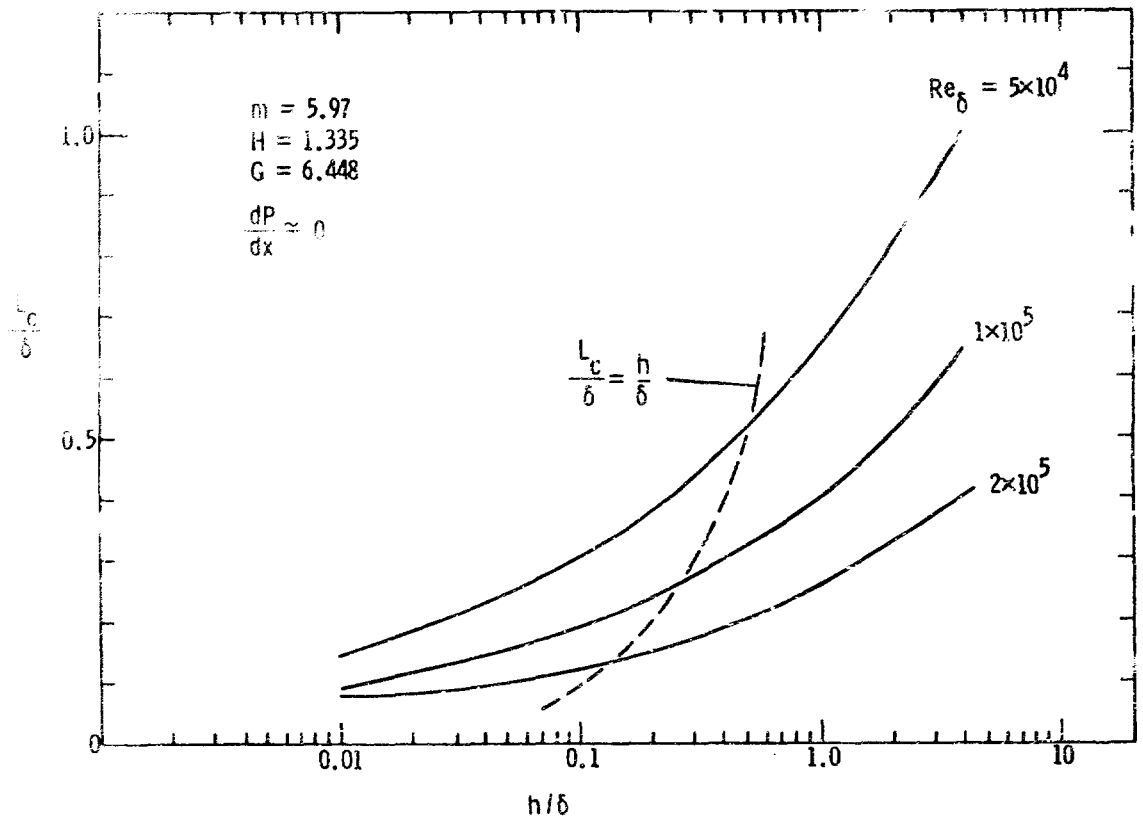

Figure 5-16. Variation of (L_c/δ) with $(\frac{h}{\delta})$ for a Triangular Protrusion, Over the Range of Parameters Corresponding to Fig. 5-8.

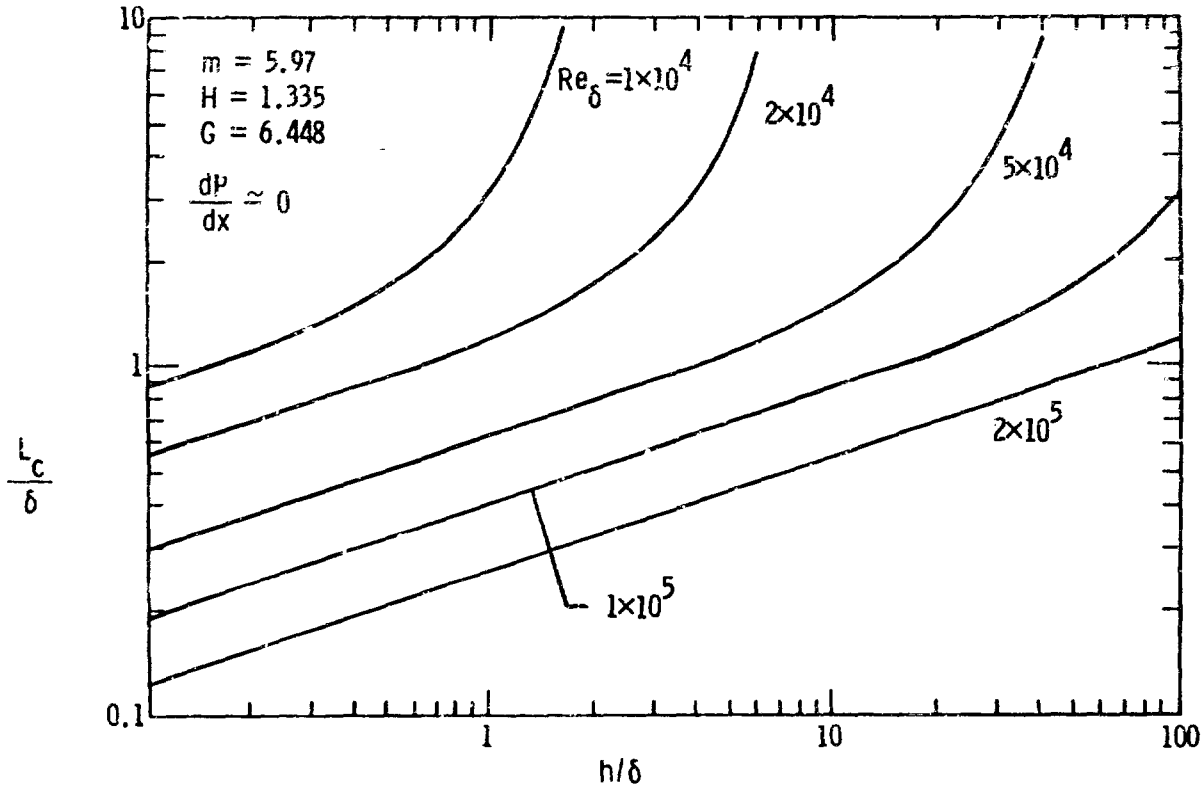

Figure 5-17. Variation of L_c/δ with h/δ for a Triangular Protrusion Over a Wide Range of Parameters.

CHAPTER VI

SUMMARY, CONCLUSIONS and RECOMMENDATION

6.1 Summary

The effect of pressure gradient on limited cavitation was experimentally investigated by using triangular protrusions.

Initially the pressure distribution was obtained in the water tunnel test section with the curved wall. Then, the velocity profiles of the boundary layer (δ) on a flat plate in the test section were measured by using a total head tube at seven stations. The nominal velocity was 40 fps.

The shape factor (G) and the wake parameter (Π) were calculated by employing the pressure gradient and the boundary layer parameters with the assistance of computer programs based on the method of E. Truckenbrodt [35]. In so doing, the values obtained by the method of E. Truckenbrodt were used for further analysis, after confirming that there was an insignificant difference between the boundary layer thickness obtained from the experiment and that obtained from the method of E. Truckenbrodt.

The limited cavitation numbers were obtained visually employing the desinence procedure over a range of free stream velocities for the various cases of zero, favorable and unfavorable pressure gradients. The maximum range of the velocity was 30 to 60 fps and the gas content was maintained less than 5 ppm during the experiment.

Finally, for the case of zero pressure gradient, the effects on limited cavitation due to the relative height and the Reynold's number

based on the boundary layer thickness were investigated. The power-law relationship between the cavitation number and the aforementioned two parameters was obtained as in Ref. [33]. In addition, a comparison of $\sigma_{\ell fp}$ versus h/δ as obtained in this investigation with that of Ref. [29], corrected to a gas content of 3.7 ppm as described in Appendix B was made to obtain a more universal relationship. Furthermore, the expression for characteristic length (L_c), used in the characteristic velocity theory, was obtained semi-empirically from the above result.

For the cases of favorable and unfavorable pressure gradients, the shape factor (G) was found as the best parameter to be related to pressure gradient. The relationship for zero pressure gradient was extended to include the influence of shape factor (G) for a flow with pressure gradient.

6.2 Conclusions

The following conclusions are based on results from the present investigations:

1. The limited cavitation characteristics of isolated roughness for a flow without pressure gradient can be represented in the form

$$\sigma_{\ell fp} = \text{constant } \left(\frac{h}{\delta}\right)^{a} \left(\frac{U_\infty \delta}{\nu}\right)^{b} \qquad (6\text{-}1)$$

where a = 0.53 and b = 0.20 were obtained from the tests of the two dimensional triangular protrusions in this investigation.

2. The power number 'a' from the current investigation was equal to 0.53 compared to a value of 0.40 obtained in Ref. [33], for a flow

without pressure gradient. The difference between the two values may be due to a difference in gas content.

3. It was reaffirmed that the characteristic velocity theory is a rough estimate of $\sigma_{\ell fp}$ for a separated protrusion element.

4. By employing a semi-empirical expression for L_c, used in the characteristic velocity theory, the theory becomes more accurate for estimation $\sigma_{\ell fp}$ for the case of a separated protrusion.

5. The effect of pressure gradient on limited cavitation for the triangular protrusion contradicts the characteristic velocity theory. This discrepancy may be due to disruptions in the local flow caused by separation from the protrusion. Separation effects are not accounted for in the characteristic velocity theory.

6. The shape factor (G) was the most consistent parameter among all others considered to be employed as a measure of pressure gradient effects on the limited cavitation number.

7. Equation (6-1) was extended for a flow with pressure gradient, to include the influence of shape factor (G), resulting in the general equation

$$\sigma_{\ell fp} = C\left(\frac{h}{\delta}\right)^{a} \left(\frac{U\delta}{\nu}\right)^{b} (G)^{e} \qquad (6\text{-}2)$$

where C = 0.0143, a = 0.53, b = 0.2 and e = 1.25 were obtained from the tests of the two dimensional triangular protrusions in this investigation. This correlation was shown to be in good agreement with experimental data. It is felt that equation (6-2) can be applied to other types of isolated roughness by varying the constants c, a, b and e, which must be obtained empirically.

6.3 Recommendations

The following is the list of recommendations:

1. Care should be taken in using equation (6-2) for predicting the cavitation characteristics of surface roughness at large values of the shape factor (G), where this relationship may not be valid. Presently, the estimations obtained with this method are in good agreement with the data for values of $G \leq 7.647$.

2. Visual observation of desinent cavitation should be carried out as far as possible at constant gas content. However, equation (5-17) may be useful for correcting for variations in gas content.

3. The cavitation characteristics of additional roughness elements, including streamlined surface protrusions, should be investigated.

4. To apply the characteristics velocity theory to other types of surface roughness, one must obtain $\sigma'_{\ell fp}$ for the particular roughness. For a roughness with separated flow, $\sigma'_{\ell fp}$ must be obtained experimentally whereas for the non-separated flow about a roughness one can obtain $\sigma'_{\ell fp}$ theoretically.

5. As indicated under item 5 in the conclusions, the discrepancy between experimental data and the characteristic velocity theory may be due to separation effects. Thus it is recommended that experiments with various pressure gradients as employed in this investigation be conducted with a protrusion which produces a nonseparated flow.

REFERENCES

1. Shalnev, K. K., "Cavitation of Surface Roughnesses," DTMB Translation, 259, 1955.

2. Walker, Jr., G.K., "Rotational Flow Over a Surface Protrusion," Master of Science Dissertation, Department of Aeronautical Engineering, The Pennsylvania State University, January 1957.

3. Holl, J. W., "The Inception of Cavitation on Isolated Surface Irregularities," Trans. ASME, Journal of Basic Engineering, Vol. 82, 1960, pp. 169-182.

4. Holl, J. W., "The Estimation of the Effect of Surface Irregularities on the Inception of Cavitation," Proceedings of Symposium on Cavitation in Fluid Machinery, ASME, 1965.

5. Benson, B. W., "Cavitation Inception on Three-Dimensional Roughness Elements," David Taylor Model Basin, Report No. 2104, May 1966.

6. Benson, D. B., "The Influence of Roughness on the Inception of Cavitation," M.S. Thesis, Massachusetts Institute of Technology, June 1958.

7. Arndt, R. E. A., "Cavitation Near Surfaces of Distributed Roughness," Ph.D. Dissertation, Department of Civil Engineering, Massachusetts Institute of Technology, June 1967.

8. Arndt, R. E. A., and Ippen, A. T., "Rough Surface Effects on Cavitation Inception," Trans. ASME, Journal of Basic Engineering, Vol. 90, pp. 249-261, 1968.

9. Messenger, H. E., "Cavitation Inception Near a Surface Roughened with Sand Grains," M.S. Thesis, Massachusetts Institute of Technology, January 1968.

10. Huber, W. C., "Cavitation Inception in Turbulent Boundary Layers Over Rough Surface," M.S. Thesis, Massachusetts Institute of Technology, January 1969.

11. Bechtel II, W. T., "The Influence of Surface Irregularities on Cavitation: Field Study and Limited Cavitation Near Wire Screen Roughness," M.S. Thesis, The Pennsylvania State University, June 1971.

12. Numachi, F., Oba, R., and Chida, I., "Effects of Surface Roughness on Cavitation Performance of Hydrofoils - Report 1," Trans. ASME, Journal of Basic Engineering, Vol. 87, 1965.

13. Numachi, F., Oba, R., and Chida, I., "Effects of Surface Roughness on Cavitation Performance of Hydrofoils - Report 2,: Symposium on Cavitation in Fluid Machinery, ASME, 1965.

14. Prandtl, L., Z. Ver. Dtsch. Ing., Vol. 77, pp. 105-114 (Trans. on NACA Tech. Mem. 720), 1933.

15. Kármán, T. von. Machr. Ges. Wiss. Goett. Math.-Phys. Kl., pp. 58-76, 1930.

16. Millikan, C. B., Proc. 5th Int. Congr. Appl. Mech., Cambridge, Massachusetts, pp. 386-392, 1938.

17. Nikuradsi, J., "Tubulente Strömung in nicht Kreisförmigen Rohren," Ing.-Arch. 1, 306-322, 1930.

18. Coles, D. E., "The Law of the Wall in Turbulent Shear Flow," 50 Fahre Grenzschichtforschung (Ed. H. Görtler & W. Tollmein), p. 133, 1955.

19. White, F. M., Viscous Fluid Flow, McGraw-Hill Book Company, New York, 1974.

20. Clauser, F. H., "Turbulent Boundary Layers in Advance Pressure Gradients," Journal Aeronaut. Sci., Vol. 21, pp 91-180, 1954.

21. Clauser, F. H., "The Turbulent Boundary Layer," Advance Applied Mech., Vol. 4, pp. 1-51, 1956.

22. Nash, J. F.,National Physics Laboratory, Aeronautical Report 1137, England, 1965.

23. Mellor, G. L. and Gibson, D. M., "Equilibrium Turbulent Boundary Layers," Journal Fluid Mechanics, Vol. 24, pp. 225-253, 1966.

24. Stratford, B.S., "An Experimental Flow with Zero Skin Friction Throughout its Region of Pressure Rise," Journal Fluid Mechanics, Vol. 5, pp. 17-35, 1959.

25. Herring, H. J. and Norbury, J. F., "Some Experiments on Equilibrium Turbulent Boundary Layers in Favorable Pressure Gradients," Journal Fluid Mechanics, Vol. 27, pp. 541-549, July 1966.

26. Coles, D. E., "The Law of the Wake in the Turbulent Boundary Layer," Journal Fluid Mechanics, Vol. 1, pp. 191-226, 1956.

27. Coles, D. E. and Hirst, E. A., Proceedings of Computation of Turbulent Boundary Layers, Vol. II, Department of Mechanical Engineering, Stanford University, Stanford, California, 1968.

28. Holl, J. W., and Treaster, A. L., "Cavitation Hysteresis," Trans. ASME, Journal of Basic Engineering, Vol. 86, 1960, pp. 199-212.

29. Holl, J. W., "The Effect of Surface Irregularities on Incipient Cavitation," Ph.D. Thesis, The Pennsylvania State University, June, 1958.

30. Holl, J. W., "The Inception of Cavitation on Isolated Surface Irregularities," Journal of Basic Engineering, Trans. ASME, Vol. 82, 1960, pp. 169-183.

31. Kermeen, R. W., and Parkin, B. R., "Incipient Cavitation and Wake Flow Behind Sharp-Edged Disks," California Institute of Technology Hydrodynamics Laboratory Report 85-4, Pasadena, Calif., August 1957.

32. Arndt, R. E. A., "Semi-empirical Analysis of Cavitation in the Wake of a Shape Edged Disk," Journal of Fluids Engineering, Trans. ASME, Vol. 98, September 1976.

33. Arndt, R. E. A., Holl, J. W., Bohn, J. C., and Bechtel, W. T., "Influence of Surface Irregularities on Cavitation Performance," Journal of Ship Research, Vol. 23, No. 3, September 1979.

34. Lehman, A. F., "The Garfield Thomas Water Tunnel," ORL Report No. Nord 16597-56, The Pennsylvania State University, 1957.

35. Truckenbrodt, E., "A Method of Quadrature for Calculation of the Laminar and Turbulent Boundary Layer in Case of Plane and Rotationally Symmetrical Flow," NACA TM 1379, May 1955.

36. Ludwieg, H. and Tillmann, W., Untersuchunger über die Wandschubspannung in Turbulenten Reibungasschichten. Ing.-Arch. 17, 288-299 (1949); summary of both paper ZAMM 29, 15-16 (1949). Eng. trans. in NACA TM 1285, 1955.

37. Abbot, I. H. and von Doenhoff, A. E., Theory of Wing Sections, Dover Publications Inc., New York, New York, 1958.

38. Billet, M. L., and Holl, J. W., "Scale ects on Various Types of Limited Cavitation," The ASME International Sumposium on Cavitation Inception, December 1979.

APPENDIX A

DESIGN OF EXPERIMENT

A.1 Curved Wall

The objective of mounting the curved wall in the water tunnel test section was to obtain various pressure gradients in the test section. The minimum pressure coefficient has to be more than -0.4, derived by the superposition equation, in order to make a successful experiment in the water tunnel because of pressure limitations.

Originally, a NACA 0013-34 airfoil was selected from reference [37]. Furthermore, the minimum pressure coefficient in this test section was derived by using a computer program. Unfortunately, the value was found to be below -0.4, so a curved wall was modified to obtain a proper value of the minimum pressure coefficient. The configuration and the pressure coefficient are shown in Fig. 4-5 and Fig. 5-3, respectively.

A.2 Triangular Protrusion

After calculating the pressure gradient, seven points were selected for locating the triangular protrusions. Three of them were located where the pressure gradient is the maximum, the minimum and zero. Four other points were selected such that two of them have the same absolute pressure gradient. The locations of the seven stations are shown in Fig. A-1.

The heights of the protrusions were selected so that the cavitation numbers for three cases within the boundary layer and for one case outside of the boundary layer could be measured. The boundary layer was

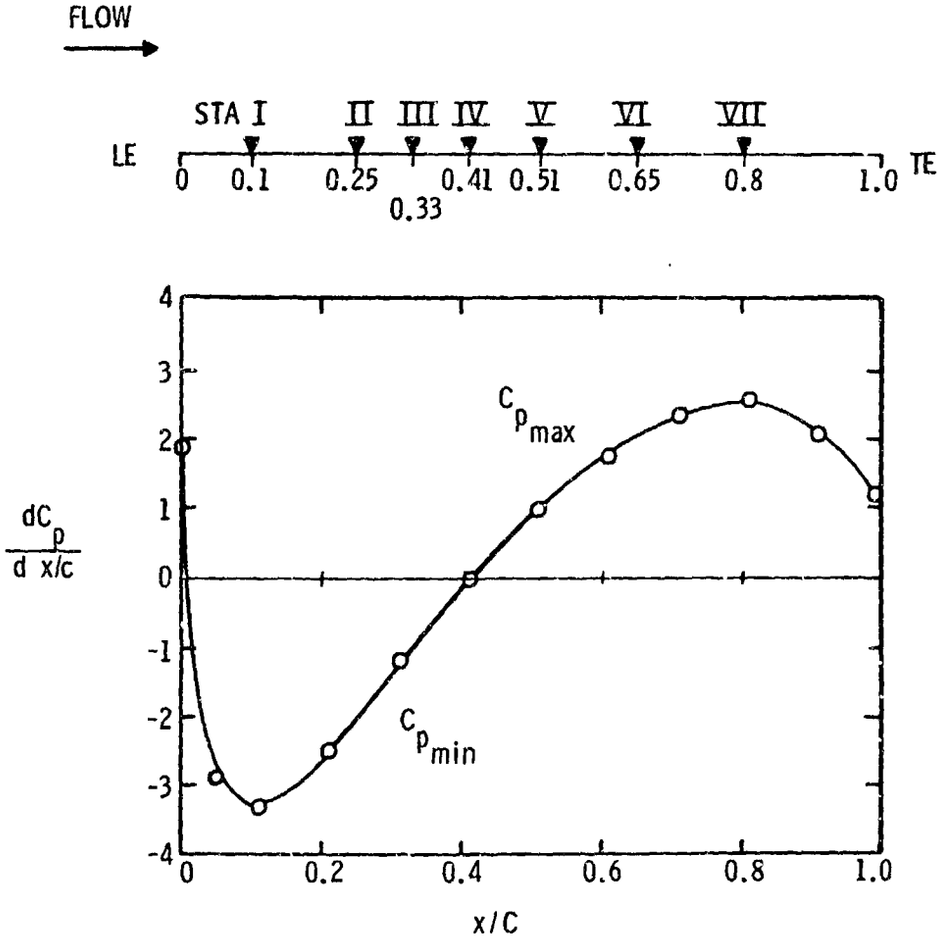

Figure A-1. Location of Triangular Protrusion Relative to Pressure Gradient.

roughly calculated by using the equation for a flat plate. The initial schedule of the experiments is shown in Table A-1.

TABLE A-1

INITIAL SCHEDULE FOR CAVITATION TEST

STA.	I	II	III	IV	V	VI	VII
δ(inch)	0.045	0.095	0.117	0.140	0.167	0.202	0.218
h(inch)							
1/100	0						
2/100	0						
3/100	0	0	0				
5/100		0	0	0	0		
7/100	0	0	0	0	0	0	0
10/100				0	0	0	0
15/100		0	0			0	0
30/100				0	0	0	0

APPENDIX B

CORRECTION OF CAVITATION NUMBER FOR A VARIATION IN GAS CONTENT

The effect of gas content for limited cavitation number has been demonstrated by Billet and Holl [38] as

$$\sigma_\ell = - C_{P_{min}} + \frac{k\alpha\beta'}{1/2\ \rho U_\infty^2} \quad , \tag{B-1}$$

where α, β' and k are the dissolved gas content (PPM), Henry's law constant (PSI/PPM) and an empirical adjustment factor, respectively. Equation (B-1) was initially proposed by Holl in Ref. [29]. For the present result and that of Ref. [29], equation (B-1) becomes

$$\sigma_P = - C_{P_{min}} + \frac{k\alpha_P\beta'}{1/2\ \rho U_\infty^2} \tag{B-2}$$

or

$$\sigma_R = - C_{R_{min}} + \frac{k\alpha_R\beta'}{1/2\ \rho U_\infty^2} \tag{B-3}$$

where the subscripts P and R stand for present and Ref. [29], respectively. By using the data of Ref. [29], which were carried out under the same condition except for the gas content, k can be expressed by equation (B-2) in the form

$$k = \frac{(\sigma_{Ra} - \sigma_{Rb})}{(\sigma_{Ra} - \sigma_{Rb})} \frac{1/2\ \rho U^2}{\beta'} \quad , \tag{B-4}$$

where the subscripts a and b are arbitrary numbers. Since these two experiments were carried out for a water temperature of approximately

72^{o}F, the Henry's law constant is

$$\beta' = 1.00 \text{ (PSI/PPM)} \quad . \tag{B-5}$$

Substituting Equation (B-5) into Equation (B-4) gives

$$k = \frac{(\sigma_{Ra} - \sigma_{Rb})}{(\alpha_{Ra} - \alpha_{Rb})} \frac{1}{2} \rho U_{\infty}^2 \quad . \tag{B-6}$$

The results are tabulated in Table B-1.

As indicated previously, since the present experiment was carried out with almost the same gas content, the mean value in the present experiment was used as α_P. Thus,

$$\sigma_P = \frac{\sum_{i=1}^{n} (\alpha_P)_i}{n} = 3.7 \text{ (PPM)} \quad . \tag{B-7}$$

The cavitation number of Ref. [29], corrected for the reference gas content corresponding to the present investigations, $\sigma_{R\text{-corr}}$ is expressed in the form of

$$\sigma_{R\text{-corr}} = \sigma_R - \frac{k(\alpha_R - \alpha_P)\beta'}{1/2 \ \rho U_{\infty}^2} \quad . \tag{B-8}$$

Employing equations (B-5) and (B-7) in equation (3-8) gives

$$\sigma_{R\text{-corr}} = \sigma_R - \frac{k(\alpha_R - 3.71)}{1/2 \ \rho U_{\infty}^2} \tag{5-17}$$

where k is 0.104.

TABLE B-1

CONSTANT (k) FOR EFFECT OF GAS CONTENT

DATA SET	h/δ	U_∞ (fps)	$(\alpha_{Ra} - \alpha_{Rb})$ (PPM)	k
1	0.0634	20	10.12	0.048
		30		0.072
		40		0.088
		50		0.091
2	0.2480	20	4.49	0.005
		30		0.030
		40		0.154
		50		0.117
3	0.2480	20	7.58	0.131
		30		0.166
		40		0.075
		50		0.286
4	0.5030	20	10.03	0.028
		30		0.067
		40		0.044
		50		0.234
		AVERAGE		0.104

DISTRIBUTION LIST FOR UNCLASSIFIED Technical Memorandum 82-218 by Masaru Tada, dated 18 October 1982

Commander
Naval Sea Systems Command
Department of the Navy
Washington, DC 20362
Attn: Library
Code NSEA-09G32
(Copies 1 and 2)

Commander
Naval Sea Systems Command
Department of the Navy
Washington, DC 20362
Attn: T. E. Peirce
Code NSEA-63R31
(Copy No. 3)

Commander
Naval Sea Systems Command
Department of the Navy
Washington, DC 20362
Attn: F. B. Peterson
Code NSEA-56X
(Copy No. 4)

Commander
David W. Taylor Naval Ship
R&D Center
Department of the Navy
Bethesda, MD 20084
Attn: Library
Code 522
(Copy No. 5)

Commander
David W. Taylor Naval Ship
R&D Center
Department of the Navy
Bethesda, MD 20084
Attn: T. T. Huang
Code 1552
(Copy No. 6)

Commander
David W. Taylor Naval Ship
R&D Center
Department of the Navy
Bethesda, MD 20084
Attn: Y. T. Shen
Code 1552
(Copy No. 7)

Commander
David W. Taylor Naval Ship
R&D Center
Department of the Navy
Bethesda, MD 20084
Attn: J. H. McCarthy
Code 1540
(Copy No. 8)

Commanding Officer
Naval Underwater Systems Center
Department of the Navy
Newport, RI 02840
Attn: Library
Code 54
(Copy No. 9)

Commanding Officer
Naval Ocean Systems Center
Department of the Navy
San Diego, CA 92152
Attn: Library
(Copy No. 10)

Commander
Naval Surface Weapons Center
Department of the Navy
Silver Spring, MD 20910
Attn: Library
(Copy No. 11)

Defense Technical Information Center
5010 Duke Street
Cameron Station
Alexandria, VA 22314
(Copies 12 through 17)

Naval Research Laboratory
Department of the Navy
Washington, DC 20390
Attn: Library
(Copy No. 18)

Office of Naval Research
Department of the Navy
800 North Quincy Street
Arlington, VA 22217
Attn: Director
(Copy No. 19)

DISTRIBUTION LIST FOR UNCLASSIFIED Technical Memorandum 82-218 by Masaru Tada, dated 18 October 1982 - continued

The Pennsylvania State University
Applied Research Laboratory
Post Office Box 30
State College, PA 16801
Attn: GTWT Files
(Copy No. 20)

The Pennsylvania State University
Applied Research Laboratory
Post Office Box 30
State College, PA 16801
Attn: J. W. Holl
(Copies 21 through 26)

The Pennsylvania State University
Applied Research Laboratory
Post Office Box 30
State College, PA 16801
Attn: M. L. Billet
(Copy No. 27)

The Pennsylvania State University
Applied Research Laboratory
Post Office Box 30
State College, PA 16801
Attn: D. R. Stinebring
(Copy No. 28)

The Pennsylvania State University
Applied Research Laboratory
Post Office Box 30
State College, PA 16801
Attn: R. E. Henderson
(Copy No. 29)

The Pennsylvania State University
Applied Research Laboratory
Post Office Box 30
State College, PA 16801
Attn: M. T. Pigott
(Copy No. 30)

The Pennsylvania State University
Applied Research Laboratory
Post Office Box 30
State College, PA 16801
Attn: B. R. Parkin
(Copy No. 31)

The Pennsylvania State University
Applied Research Laboratory
Post Office Box 30
State College, PA 16801
Attn: A. L. Treaster
(Copy No. 32)

Dr. Allan J. Acosta
Division of Engineering and
Applied Science
California Institute of Technology
Pasadena, CA 91125
(Copy No. 33)

Mr. Masaru Tada
Japan Highway Public Corporation
Machine & Electricity Section
7-2, Kohjimachi 5-Chome
Chiyoda-ku, Tokyo
Japan
(Copies 34 and 35)

Dr. S. Yokoyama
Department of Mechanical Engineering
Gunma University
Kiryu-shi, Gunma-ken
Japan
(Copy No. 36)

Dr. H. Narui
Department of Mechanical Engineering
The National Defense Academy
Hashirimizu, Yokosuka-shi
Kanagawa-ken, Japan
(Copy No. 37)